Tendencies of soil microbial NO emissions during HI-SCALE as predicted by a nitrification / denitrification scheme

B. Gaudet [1], J. Fast[1], Q. Rasool [2,3], M. Shrivastava [1], S.-L. Tai [1], R. Zaveri[1], and J. Zhang [4]

[1]Pacific Northwest National Laboratory, Richland, WA, USA
[2]Cooperative Institute for Research in Environmental Sciences, Boulder, CO, USA
[3]NOAA Chemical Sciences Laboratory, Boulder, CO, USA
[4]Lawrence Berkeley National Laboratory, Berkeley, CA, USA

Key Points:

- Microbial soil NO emissions can significantly impact modeled nitrogen / ozone chemistry over rural areas of the U.S. Great Plains.
- Soil NO emissions reduce but do not eliminate negative biases in gaseous / aerosol species when evaluated against aircraft and surface data.
- Modeled soil NO emission show seasonal dependencies based on soil moisture and temperature, but modulated by soil type.

Corresponding author: Brian Gaudet, Brian.Gaudet@pnnl.gov

Abstract

Many atmospheric chemical processes, including the formation of secondary organic aerosol (SOA), are strongly modulated by the reactions of NO and NO_2 (NO_x). Though NO_x is controlled by anthropogenic emissions near urban areas, in rural areas soil microbial nitrification and denitrification can be a significant contribution to NO emission globally. The relative rates of emissions of different nitrogen-containing species (e.g., NO, N_2O, HONO, N_2) are strong functions of soil properties such as temperature, moisture content, pH, and soil carbon and nitrogen pools. However, typical large-scale biogeochemical models either express these emissions simplistically, or not at all. Here we investigate the potential impact of soil NO emissions on atmospheric NO_x chemistry and SOA formation over regional and monthly time scales, specifically the 2016 spring and summer Intensive Observational Periods (IOPs) of the Holistic Interactions of Shallow Clouds, Aerosols and Land Ecosystems (HI-SCALE) field campaign. We implement a mechanistic soil NO parameterization into the Weather Research and Forecasting model coupled with Chemistry (WRF-Chem) model, supplemented by a 1-km soil moisture analysis. We then simulate both IOPs over the U.S. Great Plains, evaluating against ground stations and flight data. We show that soil NO emissions can account for a large fraction of total NO_x and locally increase O_3 concentrations by up to 25%, while alleviating negative biases of gases and aerosols towards observations. Meteorology and soil moisture and temperature changes between IOP1 and IOP2 lead to overall differences in emissions, but with large regional variability due to heterogeneous surface characteristics.

Plain Language Summary

Nitric oxide (NO) is a gaseous species that when emitted near the surface can have strong impacts on atmospheric chemical processes that can generate various pollutants, such as nitrogen dioxide (NO_2) and ozone (O_3), as well as aerosols that can serve as cloud droplet nuclei and hence impact cloud structure and lifetime. While NO chiefly arises from man-made sources, far away from local sources the emission of NO from soil microbes can be significant, and is thought to account for as much as 20-25% of the global total. Most models that would be used to predict atmospheric chemistry over a region such as the U.S. Great Plains over timescales of less than a few months do not take soil NO emissions into account in sufficient detail, as they are complex functions of soil temperature, soil moisture, and other surface properties. In this study we take a soil NO emission model and implement it into the widely used WRF-Chem atmospheric model. Simulations of the U.S. Great Plains over two months from a field campaign show better agreement with the observations when soil NO is included and we use a new dataset of 1-km soil moisture.

1 Introduction

Oxides of nitrogen (NO_x) including nitric oxide (NO) and nitrogen dioxide (NO_2) constitute a group of highly reactive nitrogenous gases that react with oxygen, water, and other chemicals in the atmosphere forming acid rain, and fine particulate matter (inorganic particles containing nitrate and organic particles) contributing to haze. NO_x catalyzes tropospheric ozone production and destruction and reacts with with hydroperoxyl radicals (HO_2) and organic peroxy radicals (RO_2) during the daytime forming hydroxyl radicals (OH) (Seinfeld & Pandis, 2016). OH radicals are one of the key oxidants that affect the lifetime of greenhouse gases like methane (CH_4) and cause the oxidation of Volatile Organic Compounds (VOCs) forming secondary organic aerosols (SOA). In addition to serving as atmospheric pollutants, SOA have the potential to serve as cloud condensation nuclei (CCN), which could thus affect local cloud formation and dissipation, with implications for the Earth's radiative budget.

NO_x gases are primarily emitted by the high temperature combustion of fossil and biomass fuels. However, non-combustion soil processes could also emit NO, and soil NO emissions have been reported to be the primary drivers of OH radical production in clean terrestrial locations like the Amazon rainforest (Shrivastava et al., 2019). Soil nitrogen can be converted and released as NO gases to the atmosphere through both microbial activity (through biotic/enzymatic) processes and chemical (abiotic non-enzymatic) processes (Pilegaard, 2013). In addition to the existing natural soil nitrogen, fertilizer/manure application and deposition of nitrogen from the atmosphere add to the soil nitrogen content. In urban areas, anthropogenic NO_x emitted from combustion activities (like vehicular exhaust, power plant plumes, biofuel burning) might dominate NO_x emissions; however, in agricultural regions like the northern mid-latitudes, emissions of NO_x from soil microbes can be significant (Jaeglé et al., 2005). About 22% of global surface soil NO_x emissions have been attributed to soil sources (Jaeglé et al., 2005). Soil emission of NO_x relative to other N-containing species (e.g., NH_3, N_2O, N_2, and HONO) is a function of the relative rates of nitrification / denitrification in the soil. These rates in turn are functions of various soil properties, such as pH and the ratio of microbial C to N pools, but soil moisture / water-filled pore space in soils is one of the primary drivers of these rates (Oswald et al., 2013; Rasool et al., 2019b). This dependence, however, is complicated; while there is a general tendency for NO emissions to decrease with increasing water content, after extended dry periods the presence of rain can lead to a 'pulse' of NO emissions an order of magnitude greater than the background rate (Hudman et al., 2012). Therefore, realistically predicting these soil emissions requires information about the chemical state of soil C and N pools as well as the amount and evolution of soil moisture with time.

Existing large-scale chemical models, when they do not neglect soil NO emissions altogether, tend to represent them as simple functions based on total available soil N. Yienger and Levy II (1995) developed a scheme (YL) that represents fluxes as functions of biome type modified by various factors, including temperature. Soil moisture dependence is included via dry soil / wet soil classification based on antecedent precipitation. The Berkeley-Dalhousie Soil NO_x Parameterization (BDSNP) (Hudman et al., 2012) also has biome-dependent baseline emissions of NO, but it includes both soil temperature and moisture continuous emission factors for NO. These schemes have been incorporated into the GEOS-Chem transport model (Wang et al., 1998; Hudman et al., 2012) and the US EPA's Community Multiscale Air Quality Model (CMAQ) (Rasool et al., 2016). A similar parameterization to represent soil microbial emission of HONO has been implemented into the Weather Research and Forecasting model coupled with Chemistry (WRF-Chem) (Zhang et al., 2016, 2017). Recently, Ren et al. (2025) has also run WRF-Chem including parameterizations of soil NO and HONO emissions that contain temperature- and moisture-dependent emission factors Wang et al. (2021, 2023).

In this study, we implement a mechanistic parameterization to predict soil NO emissions into the Weather Research and Forecasting model coupled with Chemistry (WRF-Chem), and use the model to simulate the U.S. Midwest region for the Apr-May 2016 and Aug-Sep 2016 Intensive Observing Periods (IOPs) of the Holistic Interactions of Shallow Clouds, Aerosols and Land Ecosystems (HI-SCALE) field campaign (Fast et al. 2019). The parameterization is derived from that of Rasool et al. (2019b), which describes the implementation of the scheme into CMAQ and its initial evaluation. The scheme is mechanistic in that different oxidation states of soil N, and nitrification / denitrification rates, are explicitly tracked, and a full range of gaseous N emission products can be predicted. We intend to evaluate the chemical field predictions of the modeling system against the HI-SCALE measurements, and evaluate the sensitivity of the modeled species to the inclusion of soil NO emissions. Because of the strong dependence of these emissions on soil properties, including but not restricted to temperature and moisture, we make use of externally generated geographical datasets that contain these properties (Rasool et al., 2019a; Tai et al., 2024) in the simulations.

Section 2 will describe our general approach and the components of our modeling system. Section 3 will then present sensitivity tests to the inclusion of soil NO emissions, an analysis of the factors leading to the modeled differences between the two IOPs, and observation verification of the baseline model simulation. Sections 4 and 5 will then include discussion of the results, conclusions, and suggestions for future work.

2 Approach

2.1 WRF-Chem

We used the Weather Research and Forecasting (WRF) model coupled with Chemistry (WRF-Chem) (Fast et al., 2006; Grell et al., 2005) version 4.2 to simulate trace gases and aerosols during the HI-SCALE IOP1 and IOP2 periods using a 12-km domain. WRF is an atmospheric regional model that can be configured with a full suite of multiple physics packages that predict land surface fluxes, cloud microphysics, turbulent mixing, and radiation (Skamarock et al. 2007).

Hourly aerosol and trace gas emissions from sources other than biomass burning and biogenic emissions are derived from the United States Environmental Protection Agency's 2017 National Emissions Inventory (NEI2017). Biogenic volatile organic compound (BVOC) emissions are derived from version 2.1 of Model of Emissions of Gases and Aerosols from Nature (MEGAN v2.1) (Guenther et al., 2012), which was recently implemented into WRF. Since the emissions from this scheme have a strong dependence on vegetation properties, the implementation occurred within the land surface model based on version 4 of the Community Land Model (CLM) (Zhao et al., 2016; Lawrence et al., 2011). In the land surface model each land use type consists of a mosaic of up to four plant function types (PFTs), for each of which BVOC emission factors are provided in Guenther et al. (2012).

Gas-phase chemistry in our WRF-Chem configuration uses the Statewide Air Pollution Research Center (SAPRC-99) mechanism, which includes 211 reactions of 74 gas phase species, 18 of which are free radicals. Inorganic aerosol chemistry and the evolution of aerosol size distribution and microphysics in WRF-Chem are represented by the Model for Simulating Aerosol Interactions and Chemistry (MOSAIC) (Zaveri et al., 2008). The MOSAIC aerosol module includes treatments of nucleation, coagulation, and condensation as described in previous studies (Chapman et al., 2009; Fast et al., 2009). In addition, both in-cloud and below-cloud wet removal of trace gases and aerosols are simulated following Easter et al. (2004). We have used SAPRC-99 coupled to MOSAIC to model gas-aerosol chemistry for simulations in multiple regions across the globe (e.g., Shrivastava et al. (2019)).

Our goal in this work is to simulate the impacts of soil NO_x emissions on atmospheric trace gas and aerosol mass concentrations across the entire period of both HI-SCALE IOPs. However, for this to be practical, we need to minimize computational resources required by the scheme. Therefore, we represent each particle-phase chemical constituent in WRF-Chem by four size sections with bin boundaries of 0.039-0.156 μm (ultrafine), 0.156 to 0.624 μm (accumulation), 0.624 to 2.5 μm and 2.5 to 10 μm, respectively, and separate particle phase tracers are used for interstitial and cloud-borne aerosols. Both particle number and mass are simulated in each bin. We represent both primary organic aerosols (POA) and secondary organic aerosols (SOA) in WRF-Chem using the simplified and computationally efficient two-species volatility basis set (VBS) treatment (Shrivastava et al., 2011) to account for the role of organics affecting aerosols and clouds. We treat the condensation/evaporation of SOA using a dynamic gas-particle partitioning approach wherein the model calculates the condensation/evaporation of organic gases using a semi-implicit Eulerian approach with adaptive time (Zaveri et al., 2014).

2.2 Soil NO scheme

To compute the natural soil fluxes of nitrogen species into the atmosphere, the mechanistic scheme of Rasool et al. (2019b) was implemented into the CLM land surface model within WRF because, like BVOCs, these emissions are strongly dependent on land surface properties. The scheme essentially consists of two components: the first tracks the amount of soil microbial NH_4, NO_3, and labile Cfor non-agricultural regions; the second predicts nitrification / denitrification rates and the gaseous emissions of NO, HONO, and N_2O that result from the soil microbial pools of C and the different forms of N.. The nitrification / denitrification framework is based on the Daily version of CENTURY model (DayCENT) biogeochemical scheme (Parton et al., 2001).

For non-agricultural regions, the USGS land use types specified in the WRF Preprocessing System (WPS) (Global Land Cover Characterization v2 from 1992-1993) are mapped to the soil biome types of Rasool et al. (2019b), which tabulates soil microbial to organic C and N fractions and HONO emission factors for each biome. These are supplemented with offline geographical datasets from Rasool et al. (2019a) which provide total soil organic carbon and nitrogen pools, microbial carbon-to-nitrogen ratios, and soil pH. From all these the soil NH_4 and labile C pools that result from the microbial life cycle are calculated as in Rasool et al. (2019b), which is based on the C / N cycling framework of Schimel and Weintraub (2003).

For agricultural regions, as in Rasool et al. (2019b), we make use of an offline simulation of the Environmental Policy Integrated Climate (EPIC) agricultural ecosystem model to create daily output of the pools of soil NH_4, NO_3, and labile C during the HI-SCALE IOPs. These pools are then incorporated into the WRF-Chem initial conditions for each simulation segment. Since these agricultural pools are predicted externally to WRF-Chem, their amounts are not re-computed within a WRF-Chem simulation.

During the WRF-Chem simulation, rates of nitrification and denitrification are computed from the soil microbial NH_4, NO_3, and labile C, treating the non-agricultural and agricultural pools separately. These rates are used to predict the evolution of the non-agricultural NH_4 and NO_3 pools as well as their emissions of the different nitrogen gaseous species. For agricultural regions, the different soil pools are prescribed externally and hence not modified, but the nitrification / denitrification rates are still computed in order to determine the agricultural nitrogen gas emissions. The nitrification / denitrification rates are based on the static soil properties and soil moisture and temperature values over the top 10 cm of the soil (the CLM levels are about 0.71 cm, 2.79 cm, 6.23 cm, 11.9 cm, 21.2 cm, 36.6 cm, 62.0 cm, 1.038 m, 1.728 m, and 2.865 m; thus, soil temperature and moisture values are averaged over the top three soil levels for this computation).

The dependencies of NO emissions from the scheme on soil temperature and moisture are complex; their relations are given in the appendix. To summarize, the nitrification rate has a linear dependence on soil temperature above 5 C, while the denitrification rate increases with temperature between asymptotic values at 0 and 30 C. Nitrification rates are also a function of volumetric soil moisture content that peak at intermediate values, depending on the values of the wilting point and field capacity for the soil type. Denitrification rates depend on the water-filled pore space (WFPS) of the soil, which is given by the ratio of volumetric soil moisture to saturated volumetric soil moisture. In addition, the ratio of NO_x to N_2O generated is modeled as a function of soil gas diffusivity, which also depends on WFPS.

For WRF land use types, it is assumed that both agricultural and non-agricultural areas can exist within a grid cell, with an agricultural fraction consistent with the fraction of the crop PFT for that type (85% for crop, 50% for crop / natural mosaic, and 0% for other types). The rates of emission of NO, N_2O, and HONO for nitrification and

denitrification are then determined for agricultural and non-agricultural regions separately. The total emission for a grid cell is found by summing the agricultural and non-agricultural emissions, weighted by the agriculture fraction. Nitrification can produce all three species, with the emissions of HONO relative to NO peaking at water-filled pore space = 0.1, while denitrification produces NO and N_2O. For both, the relative rate of NO to N_2O emission is a specified function of diffusivity.

2.3 HI-SCALE

The Holistic Interactions of Shallow Clouds, Aerosols and Land Ecosystems (HI-SCALE) field campaign (Fast et al., 2019) was supported by the Atmospheric Research Measurement (ARM) program in order to provide extensive measurements over the U.S. Great Plains to increase understanding of the life cycle of shallow clouds. During two IOPs (IOP1: 24 Apr - 15 May 2016; IOP2: 28 Aug - 21 Sep 2016), Gulfstream-159 (G-1) aircraft performed a series of flights equipped with meteorological and chemistry instrumentation. The flights were conducted in the proximity of the ARM Southern Great Plains (SGP) Central Facility, and supplement the existing long term meteorological, radiation, and chemical measurement made at that site. More information on HI-SCALE can be found in Fast et al. (2019).

In order to perform observational verification of surface chemistry measurements in the Great Plains but outside of the HI-SCALE focus region, we made use of the network of U.S. Environmental Protection Agency (U.S.-EPA) hourly surface measurements of chemical species (NO_2 and O_3), and daily measurements of nitrate (NO_3^-) aerosol concentration.

2.4 Soil moisture analysis

Because of the importance of the dependence of soil N species on soil moisture, we wanted to use make use of a high resolution soil moisture product that was observationally constrained. Towards that end, we made use of the 1-km soil moisture product found at Tai et al. (2024) and described in Tai et al. (2025). This product was generated by assimilating the 9-km Soil Moisture Active Passive mission (SMAP) soil moisture data into the Noah-MP land surface model. The SMAP soil moisture data assimilation is accomplished under the framework of NASA's Land Information System using the ensemble Kalman filter (EnKF) algorithm. 12 ensemble members were initialized by perturbing the selected variables in meteorological forcing data (the North American Land Data Assimilation System Phase 2 (NLDAS-2) (Xia et al., 2012) along with the NCEP Stage IV Quantitative Precipitation Estimate). The dataset has a spatial coverage over much of the east CONUS and is valid in the frequency of 6 hours throughout the entire year of 2016. Observational evaluation of the dataset revealed it had superior skill metrics compared to other soil moisture analyses for independent in situ soil moisture data in the U.S. Great Plains (the OK Mesonet), with RMSE values of 0.087 m^3m^{-3}. Further details on the soil moisture product including the results of evaluation using in-situ observations can be found in Tai et al. (2025).

2.5 Experimental WRF-Chem configuration

The simulations used a single 240 x 240 horizontal domain at 12 km grid spacing, encompassing most of the central U.S. and parts of the southeastern U.S. (Figure 1). As previously mentioned, the CLM land surface model, adapted for BVOC and soil NO emissions, was used for this study. Other physics options used for the simulations can be found in Table 1.

The meteorological initial and boundary conditions were derived from the 3-km High-Resolution Rapid Refresh (HRRR) analyses (Dowell et al., 2022), as well as target fields

Table 1. WRF physics options used in this study.

Physics	Option	Reference
Land Surface Model	Community Land Model (CLM)	Lawrence et al. (2011)
Planetary Boundary Layer	Yonsei University (YSU)	Hong et al. (2006)
Convective Parameterization	Modified Kain-Fritsch	Berg et al. (2015)
Radiation	Rapid Radiative Transfer Model for GCMs (RRTMG)	Iacono et al. (2008)
Microphysics	Morrison two-moment	Morrison et al. (2005)
Nudging	Above boundary layer only	Stauffer and Seaman (1990)

used for nudging the simulations. However, the soil moisture values provided by default with the HRRR land surface model were replaced by those in the high resolution soil moisture product of Tai et al. (2024) using a nearest-neighbor approach. Vertical interpolation is performed from the four levels of the soil analysis product to the finer resolution CLM soil levels. Horizontally, the high resolution soil moisture values are mapped to the WRF grid using a nearest neighbor approach. The CAM-chem global model (Emmons et al., 2020) provided initial and boundary conditions for trace gases and aerosols.

We performed simulations encompassing most of both HISCALE IOP1 (24 Apr - 15 May 2016) and IOP2 (28 Aug - 21 Sep 2016) in a series of three-day segments. Two simulations were performed for each period, one with soil emissions turned on (henceforth simulation SNOx), and one without soil emissions (henceforth simulation NoSNOx); otherwise, the configurations were identical, and as described above. While the meteorology was refreshed from HRRR after every simulation segment, the trace gases and aerosols were cycled from the previous simulation segment. The meteorology was nudged during each segment towards the 3-hourly HRRR fields above the simulated boundary layer. This procedure allows the simulated large-scale meteorology to remain tightly constrained to the HRRR analyses throughout each IOP, but allows the shorter-timescale processes within the boundary layer to be evolved by WRF unconstrained. Model output was generated every three hours, but was regenerated every 30 minutes for use the validation against HI-SCALE flight data.

3 Results

3.1 Species sensitivity to soil NO

Next, we show time series of area-averaged soil NO emissions from simulation SNOx (Figure 2). Because we are primarily interested in the integrated effect of these emissions in the rural areas of the U.S. Great Plains, we perform our area average over the domain subset corresponding to the U.S. Midwest, which we henceforth define as between longitudes 105.5 and 79.0 W, and between latitude 30.0 N and the north boundary of the model domain (yellow square in Figure 1). We can see that these emissions average range from about 5-30 g N m^{-2} hr^{-1}, but are on average higher in IOP2 than IOP1, and tend to be greatest in late afternoon, and least around dawn. A multi-scale variability dur-

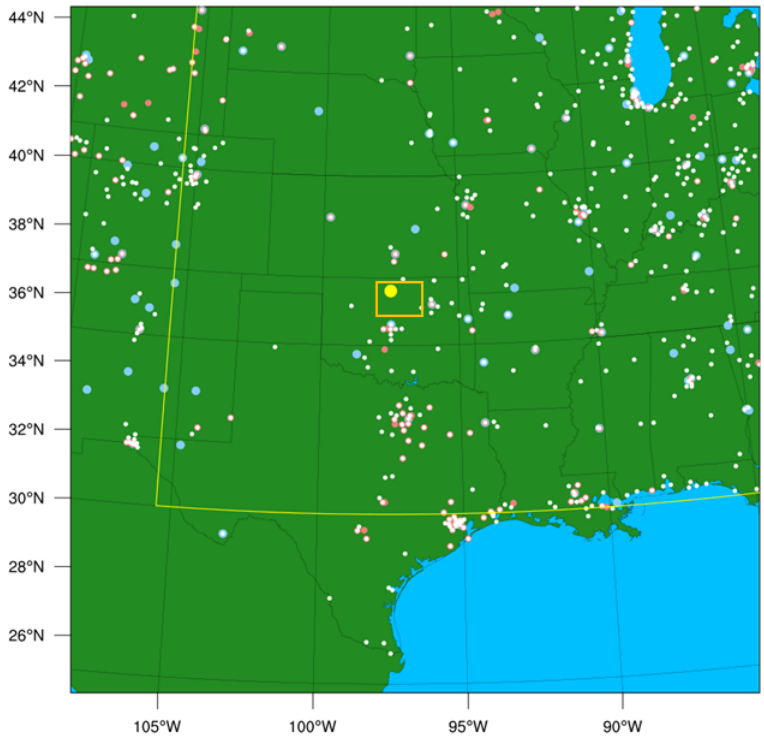

Figure 1. WRF-Chem domain used for simulations. Yellow circle indicates location of SGP Central Facility, while yellow square indicates definition of 'Midwest' region in model sensitivity analyses. Orange box indicates approximate extent of HI-SCALE aircraft coverage. EPA surface stations used for evaluation of ozone, NO_2, and nitrate concentrations are shown in white, salmon, and blue circles, respectively.

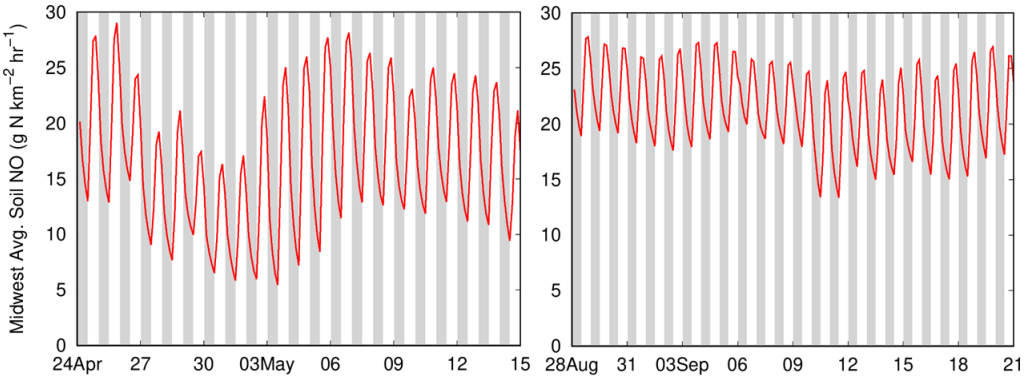

Figure 2. Time series of the IOP1 Midwest-averaged soil NO flux for IOP1 (left) and IOP2 (right) in the SNOx simulation. Periods during nighttime are shaded gray.

ing IOP1 is evident that is presumably due to synoptic weather variability, whereas the values during IOP2 are more consistent day-to-day.

Now, we examine Midwest-averaged time series of the concentration differences of various species between the SNOx and NoSNOx simulations. In Figure 3 we show a vertical profile of the soil / no-soil difference in NO_x concentration across both IOPs, along with three time series at the lowest model level, consisting of the actual NO_x concentration for each simulation, the concentration difference, and the fractional concentration difference. For IOP1, we see that the Midwest domain-averaged NO_x concentration at the lowest model level can change by up to 2 ppb through the inclusion of soil emissions, which can represent a nearly 100% increase in the overall amount at these times. The diurnal cycle of the soil NO_x contribution is closely correlated with the total NO_x concentration, which tends to peak in the nighttime hours; the diurnally-averaged fractional change in concentration is on the order of 50%.

The nighttime concentration maxima for these species reflects shallower boundary layer depths and less vertical mixing under these conditions, as can be seen by the domain-averaged boundary layer heights in panels a and d. However, a small but noticeable portion of soil-emitted NO_x is evidently transported from the daytime boundary layer to the free troposphere; the concentration plumes in the free troposphere appear to ascend from the peak boundary height towards a maximum height 6-12 hours later. This implies an ascent rate of a few to up to 10 cm s^{-1}; this conceivably could be due to transport by strong synoptic systems, but at the stronger end probably reflects convective transport. In any event, it suggests that soil NO emissions can have some impacts at large horizontal distances from the initial source region.

Superimposed on the general trend of higher nighttime NO_x concentrations are two peaks at the beginning and end of night in simulation NoSNOx, corresponding to anthropogenic emissions from the evening and morning rush hours. These subsidiary peaks are also visible in simulation SNOx, but since the soil emissions do not exhibit this behavior, the relative prominence of these peaks is reduced. Meanwhile the daily maximum NO_x concentration attributed to soil NO emissions exhibits variability on a multi-day

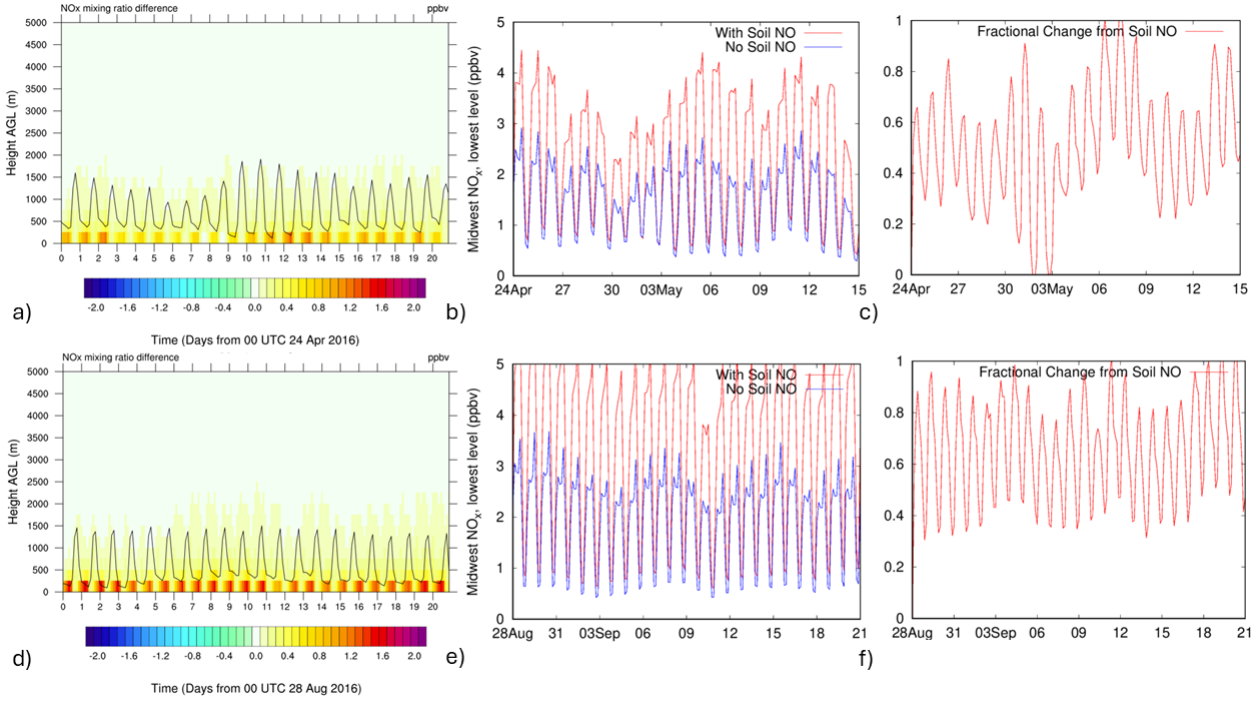

Figure 3. (Left column). Time series of the Midwest-averaged NO_x concentration differences between the SNOx and NoSNOx simulations as function of height. Black line indicates Midwest-averaged PBL height. (Middle column) Time series of Midwest-averaged NO_x concentrations at lowest model (about 19 m AGL) for SNOx and NoSNOx simulations. (Right column) Time series of Midwest-averaged fractional NO_x concentration differences. Top row is IOP1, bottom row is IOP2.

timescale that is positively correlated with the variability of soil NO emissions themselves, as shown in Figure 2.

Similar patterns appear for IOP2, but both the daily maximum soil NO_x contributions and the total NO_x contributions are even greater, being increased by approximately 50%. There does seem to be less multi-day variability in the daily maxima than in IOP1. Both of these are consistent with the trends of soil NO emissions during IOP2.

In Figure 4, we show the impact of these emissions on ozone. The percent impact on O_3 is less than on NO_x, about 5% on average in IOP1 and 10% for most of IOP2, which might be expected since it is not a direct emission product. However, this still represents a regional average of up to 2-5 ppb each day, which can be a significant contribution to non-attainment of EPA emission standards. As with NO_x, time of peak fractional impact of soil NO emissions on O_3 coincides with the time of maximum concentration, which in this case is in the late afternoon local time.

As with NO_x, we also see some evidence of ozone transport to the free troposphere after the peak of boundary layer height. This transport might appear more prominent than was the case for NO_x because for ozone peak concentration and peak boundary layer height happen to be correlated in time. But it might also reflect longer lifetimes for O_3, which allow concentration signals from the boundary layer to persist over greater depths and distances.

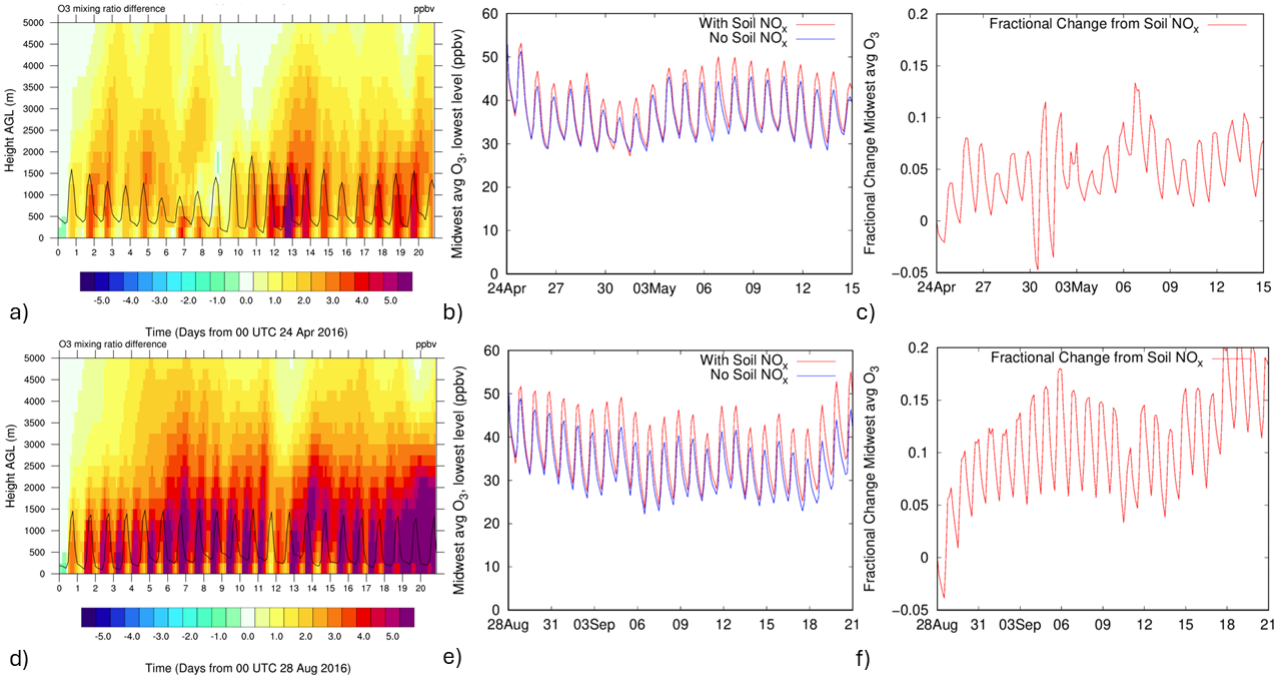

Figure 4. Same as Figure 3, but for O_3.

3.2 Spatial maps of species sensitivity

Domain-wide spatial averages of species concentrations may underestimate their sensitivity to soil NO emissions in particular regions, such as in rural areas where the relative importance of these emissions is greater. In Figure 5 we show the spatial pattern of NO_x and O_3 concentration differences and percent changes averaged across all 3-hr output times for both IOPs. We see that the spatial patterns of the greatest NO_x enhancements are similar for IOP1 and IOP2 but generally greater in IOP2, approaching 5 ppb at locations in the western U.S. Great Plains. For O_3, the same tendency occurs, with maximum enhancements approaching 10 ppb for IOP2. However, the pattern of O_3 enhancements are more widespread and uniform than those of NO_x, probably from to the greater importance of transport to O_3 concentrations due to its greater atmospheric lifetime.

The panels showing percentage changes of NO_x and O_3 from soil NO emissions demonstrate their increased importance over rural vs. urban areas; patches of low percent changes of NO_x can be seen over the main urban areas in the western part of the domain (e.g., Dallas-Fort Worth, Oklahoma City, Tulsa). However, the large scale patterns are dominated by an east-west gradient, with values near 100% prevailing in the west, but mostly 20% or less in the east. Since the large-scale west-east gradient of the actual background concentration is not as prominent, the implication is that non-soil sources of NO (i.e., anthropogenic) create higher concentrations of NO_x in the eastern domain than in the west, so the fractional change caused by soil NO is reduced there. The details of the pattern though would be expected to depend on the transport for these particular seasons and could vary from year to year. For O_3 the fractional concentration changes from soil NO do not show much of an urban / rural signal, which again might reflect the increased importance of transport to O_3 concentrations averaged over this timescale.

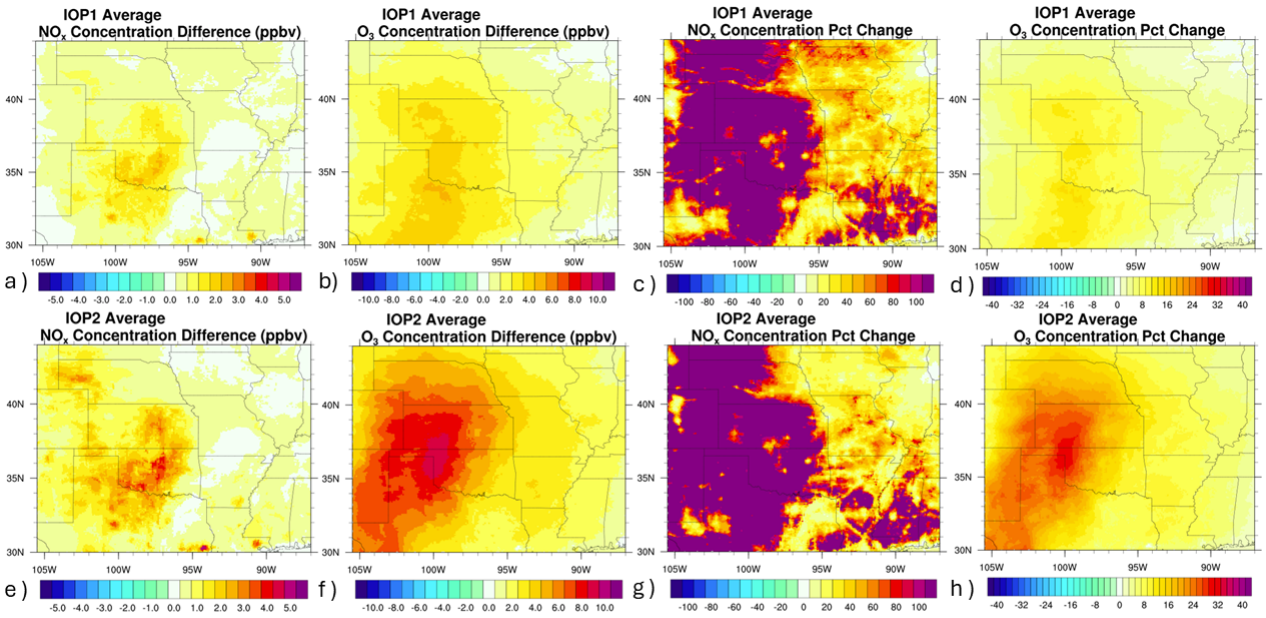

Figure 5. NO_x (a,c,e,g) and O_3 (b,d,f,h) concentration differences (a,b,e,f) and percent changes (c,d,g,h) averaged across all 3-hour output times for IOP1 (a,b,c,d) and IOP2 (e,f,g,h). Values are for lowest model level (about 19 m AGL).

3.3 Soil NO emission seasonal trends

We now examine some of the characteristics that account for the increased emissions in IOP2 vs. IOP1 in more detail. In Figure 6 we average the soil NO emissions for each IOP as a function of UTC hour. As suggested by the previous time series, emissions have a strong diurnal signal, tending to peak early-mid afternoon local standard time (Central Standard Time = UTC - 6). Here we also separate the agricultural emissions from the non-agricultural emissions. The agricultural emissions are defined as emissions from grid points that possess a crop or crop-mosaic land use type in the model, and for these points we use the offline-generated soil C and N pools to compute emissions; emissions from points with other land use categories that use WRF-Chem generated pools are defined as non-agricultural emissions. We see that the non-agricultural grid points actually have more emissions on average than the agricultural grid points, and have more diurnal variability. They are also responsible for the greater overall emissions in IOP2 vs. IOP1.

While these NO emission rates are consistent with broad range of values reported in the literature (e.g., Rasool et al. (2019b) Figure 3; Wang et al. (2023)), the reduced rates of the agricultural emissions relative to the non-agricultural emissions are a bit puzzling, although it is evidently related to the relative magnitudes and behavior of the agricultural vs. nonagricultural pools of C, NH_4, and NO_3 because both are subject to the same nitrification / denitrification scheme. It is not clear at present if there is an issue with the parameterization, or with the offline pool predictions. However, because we are interested in the sensitivity of soil NO emissions inline within WRF-Chem to soil temperature and moisture, and how this can explain the IOP1 / IOP2 emission difference, we therefore focus our remaining analysis on the non-agricultural grid points.

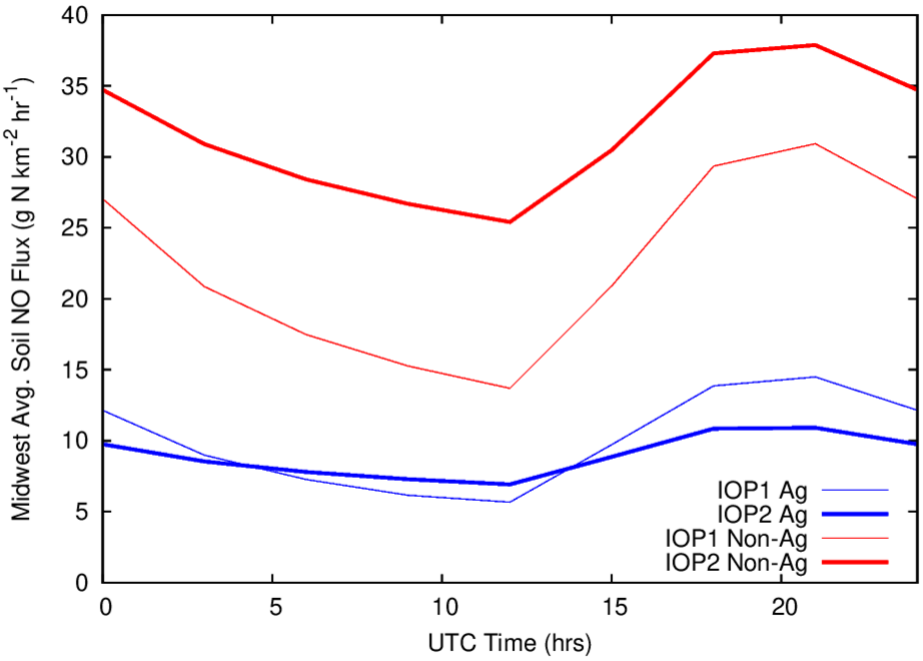

Figure 6. Emissions of soil NO averaged over each UTC hour in diurnal cycle and the Midwest region for IOP1 and IOP2. 'Ag' and 'Non-Ag' represent contributions from all the model grid points with agricultural and non-agricultural classifications.

In the soil parameterization NO emissions are a function of soil temperature, soil moisture, and other factors that are a fixed function of geography. In Figure 7 we bin all the Midwest domain points for every 18 UTC time in each IOP simulation period as a function of top level soil moisture and soil temperature, and then display the average soil NO flux emitted by all those bins, along with the joint normalized PDF of occurrence. We only include 18 UTC points to exclude the impact of the large diurnal cycle, and because this is close to the time of maximum soil NO emissions. We can see a trend of NO emissions increasing with temperature up to approximately 310 K; points with higher temperatures tend to have low soil moisture values as well as low emissions. Otherwise we also see a trend of increasing emissions with decreasing soil moisture – except for a set of points between about 0.25 - 0.35 volumetric soil moisture and $>$ 305 K with abnormally high emissions.

If soil moisture and temperature were the only influences on emissions in the scheme, the color shading in the two panels in Figure 7 would look the same. While they are quite similar, a few differences do appear; e.g., emissions around 0.25 volumetric soil moisture and 300 K are a bit higher in IOP2 than IOP1, and points with very low soil moisture emit substantially more in IOP1 than in IOP2. Since the remaining controlling factors are geographical and hence the same in IOP1 and IOP2, the panel differences can be attributed to compositional effects; i.e., the locations that are near (0.25,300) in IOP2 have traits that cause them to emit somewhat more in these conditions than the locations near (0.25,300) in IOP1.

When we examine the PDF contours in Figure 7, we find, as might be expected, the late summer IOP2 has more warmer and drier points than the spring IOP1, both of which could be expected to contribute to greater emissions in IOP2. The mode for IOP2

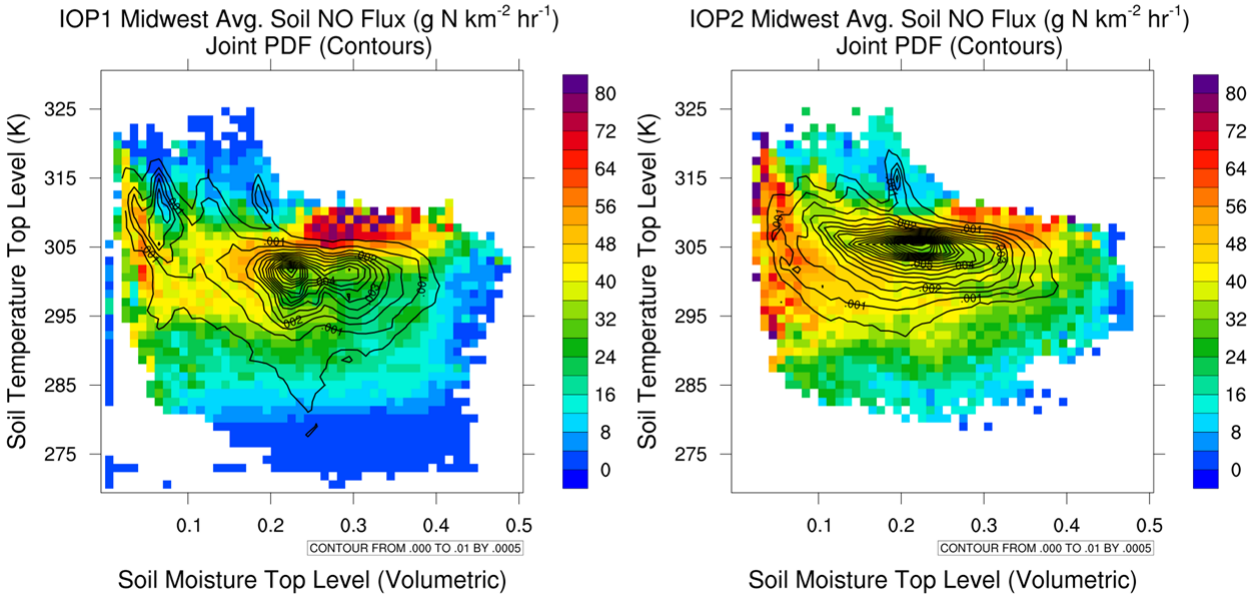

Figure 7. Heat map of emissions of soil NO (color fill) and joint PDF (contours every 0.0005) as a function of top level soil moisture and temperature, averaged for the Midwest non-agricultural points across all 18 UTC times for IOP1 (left panel) and IOP2 (right panel).

is around 305 K, vs. 302 K, and IOP2 has many more points in this temperature range with volumetric soil moisture between 0.1 and 0.2. In contrast, IOP1 has more points below 295 K, which have low emissions. But it should be noted that on close examination the immediate region of the mode emits about the same on average in both IOP1 and IOP2 (30 - 40 g N $km^{-2}hr^{-1}$).

The product of the PDF with the soil emission function in Figure 7 gives the contribution of each point in soil moisture / temperature space to the total flux (Figure 8). A comparison to Figure 7 reveals that the greater emissions in IOP2 could be adequately explained by a reduced number of low emitting points with T < 295 K, and increased number of warmer / drier points near the PDF modes, which dominate the total soil NO flux. However, Figure 7 also shows that the areas of highest emission in moisture / temperature space are well outside of the modes of the joint PDFs, so while these areas don't contribute much to the total flux, they might make a greater relative contribution to the IOP2 - IOP1 flux difference. In Figure 9, we plot the cumulative probability distribution of all the points binned by local emission for each IOP, and the contribution of each bin to that total. It can be seen that about 30% of the total emissions of IOP1, and 40% of IOP2, come from locations that emit more than 80 g N km^{-2} hr^{-1}. Furthermore, more than half of the IOP2 - IOP1 flux difference is from points that emit more than 80 g N km^{-2} hr^{-1}, which is well above the mean emission value across the whole joint moisture / temperature PDF. What this indicates is that a few locations with favorable geographical characteristics generate are high emitters and generate a large portion of the flux for each point in Figure 7.

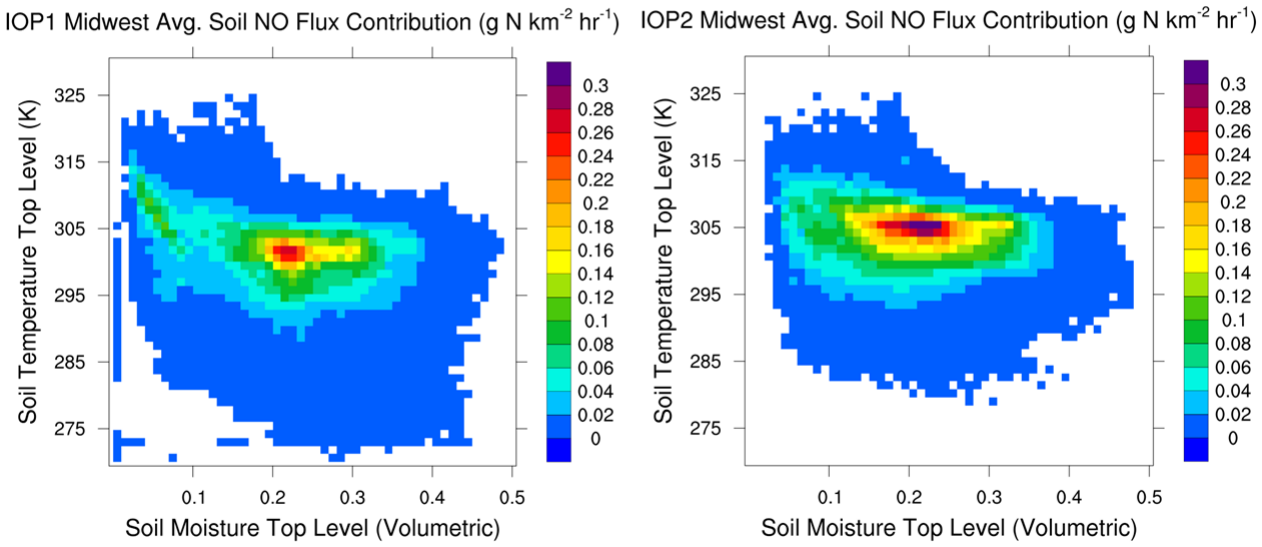

Figure 8. Contribution of each point in Figure 7 to the total soil NO flux, for IOP1 (left panel) and IOP2 (right panel).

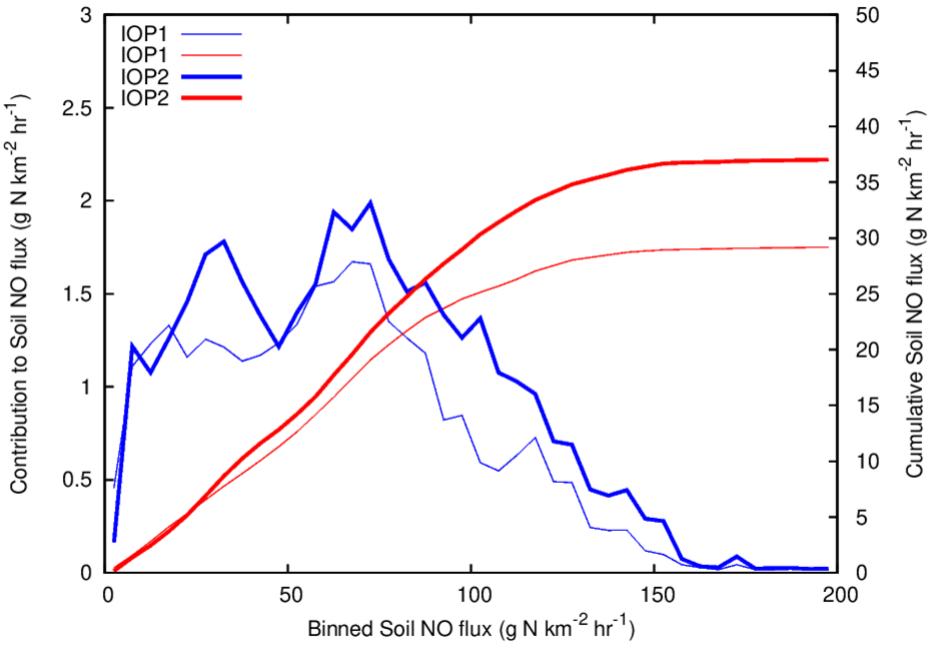

Figure 9. Cumulative soil NO flux in Midwest region as function of soil NO flux bin (right axis, red curves), and contribution to cumulative flux from each bin (left axis, blue curves) for IOP1 (thin lines) and IOP2 (thick lines).

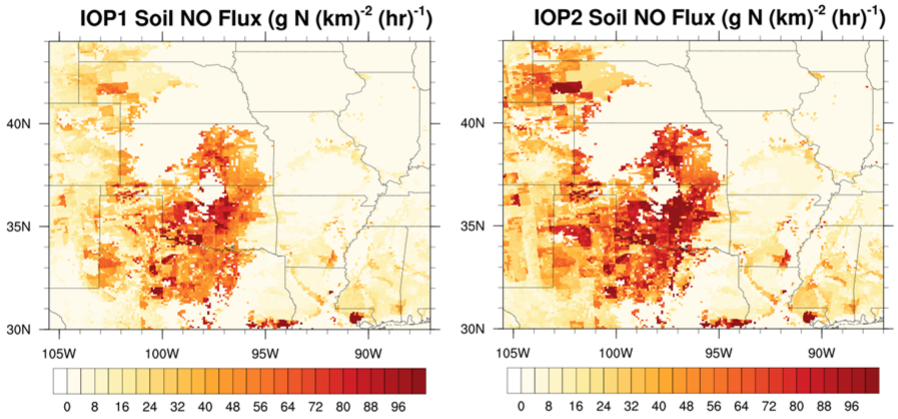

Figure 10. Geographical plot of soil NO flux averaged every 3 hours during IOP1 (left panel) and IOP2 (right panel) for non-agricultural points.

3.4 Soil NO emission seasonal sensitivities

We now look at the spatial maps to better characterize the properties of soil emissions across the two IOPs and what other factors they might depend on. Figure 10 shows the average of the soil NO emissions of simulation SNOx at each non-agricultural point during the two IOPs across all output times. The tendency for more emissions during IOP2 is discernible across most of the domain, but the high spatial variability of the emissions can also be seen. The patches generally correspond to the carbon / nitrogen pool sizes from the geographical database, modified by soil moisture and temperature. When averaged over all Midwest non-agricultural domain points, the IOP2 soil NO fluxes are 37.31 g N $km^{-2}hr^{-1}$ vs. 29.36 $km^{-2}hr^{-1}$ for IOP1.

The differences in top-level soil moisture and temperature between IOP1 and IOP2 are shown in Figures 11. As might be expected, IOP2 is generally warmer everywhere than IOP1 (domain average 302.43 K vs. 298.54 K), though the amount of warming is greater in the north than in the south. The patterns in soil moisture have more spatial variability than for soil temperature. While most of the domain appears drier in IOP2 (domain average volumetric soil moisture 0.234 in IOP2 vs. 0.247 in IOP1), exceptions do appear, particularly in the southwest near the Texas / New Mexico border, which was abnormally dry in IOP1.

When we look at pointwise correlations among IOP2 - IOP1 differences in soil NO fluxes, moisture, and temperature, as shown in the top row of Table 2, we find a seemingly contradictory result; while in the domain averages we had positive IOP2 - IOP1 soil NO fluxes associated with positive temperature and negative soil moisture differences, pointwise changes in soil NO fluxes between the two IOPs are actually *negatively* correlated with temperature changes and *positively* correlated with moisture changes. This

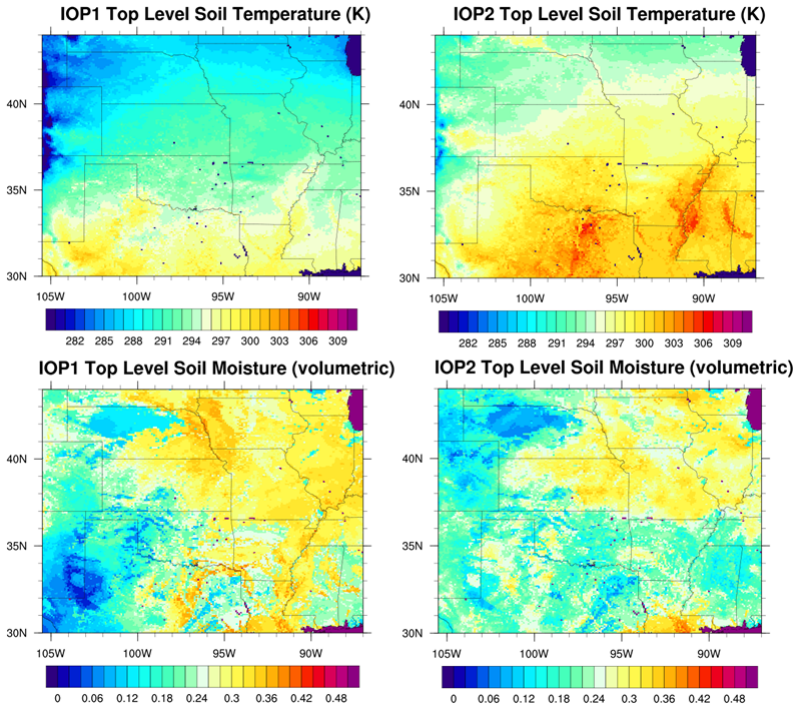

Figure 11. Same as Figure 10, but for top-level soil temperature (top row), and top-level soil moisture (bottom row).

puzzling result is a sampling compositional effect that may be explained by sorting the gridpoints by soil textural class, as is done in the rest of Table 2.

First, it can be seen that there is a strong anticorrelation of soil moisture and temperature regardless of soil texture. Physically, this can be attributed to the reduced ability of solar heating to increase the soil temperature when the soil moisture is increased. For soil types 1-4 (roughly speaking, more sandy), we see that soil NO emissions are negatively correlated with soil moisture differences, and (except for silt loam) positively correlated with temperature differences. However, for soil types 6-12 (roughly, more clay-based), we see the opposite correlations of soil NO emissions with soil temperature and moisture. Since in the parameterization the soil emissions increase monotonically with temperature when all else is equal, we conclude that for these soils the negative correlation of emissions with temperature is due to them being in a state where there is a positive correlation between emission and soil moisture, which more than counteracts the temperature dependence.

For a graphical view, we show a heat map of NO emissions as a function of soil moisture and temperature, similar to Figure 7, except now the quantities are IOP2 - IOP1 differences, and all times are now used in the average (Figure 12, top row). We also show the analysis separately for soil types 1-4 and 6-13. The all-soil figure shows negative flux differences in the top-left quadrant of positive soil temperature / negative soil moisture differences, and positive flux differences in the bottom-right quadrant, reflective of the first row of Table 2. Also visible is that the more clay soils have this same pattern while the more sandy soils have the opposite pattern. The clay soils seem to govern the all-soil pattern in the top row because at both extremes they have somewhat greater sensitivities to soil moisture / temperature changes than the sandy soils.

Table 2. Model soil properties averaged across all non-agricultural Midwest gridpoints. Columns 2-4 are correlation coefficients between top-level soil temperature and soil moisture (r_{TM}), soil NO flux and soil moisture (r_{FM}), and soil NO flux and soil temperature (r_{FT}), respectively.

Soil Texture Class	r_{TM}	r_{FM}	r_{FT}	Number
All	-0.891	0.150	-0.173	17883
1 (sand)	-0.948	-0.718	0.681	1615
2 (loamy sand)	-0.317	-0.684	0.258	243
3 (sandy loam)	-0.919	-0.490	0.468	5116
4 (silt loam)	-0.682	-0.202	-0.067	4086
6 (loam)	-0.937	0.336	-0.373	3399
7 (sandy clay loam)	-0.987	0.787	-0.818	8
8 (silty clay loam)	-0.880	0.500	-0.437	871
9 (clay loam)	-0.944	0.811	-0.853	1261
11 (silty clay)	-0.740	0.612	-0.675	280
12 (clay)	-0.880	0.744	-0.752	997
13 (organic material)	0.054	0.249	0.956	7

When we look at the PDFs (Figure 12, bottom row), we see that the peak of the distribution is in the top left quadrant relative to the origin, again consistent with IOP2 being generally warmer / drier than IOP1. However, we also see that this peak largely reflects the sandy soils, while the clay soil PDFs have a relatively greater tendency to be in the bottom-right quadrant. For each soil group these locations are those that are associated with increased soil NO emissions. Thus when we take the product of the top row with the bottom row to find contributions to the total IOP2 - IOP1 flux difference (Figure 13), we can see how the overall positive flux difference is consistent with a PDF in the warmer / drier top left quadrant.

An obvious question is why the trends of soil NO fluxes vs. temperature and moisture are opposite for the more clay and sandy soils. One feature of the more clay-based soils is that their wilting point tends to be higher. As shown in the appendix, the nitrification rates of the scheme increase most rapidly with soil moisture near the wilting point. Thus for the clay-type soils a positive correlation between soil moisture and emission is more likely (with a negative correlation between soil and emission the consequence of the negative soil temperature / moisture correlation). However, for more sandy soils the soil moisture dependence of emission is less significant, so soil emission would be controlled by the soil temperature dependence.

3.5 Observational Verification

Now that the behavior of the soil NO parameterization has been examined as a function of season and soil properties, we now evaluate the WRF-Chem predictions with aircraft observations taken during the spring and summer IOPs of the HI-SCALE field campaign (refer to the orange box in Figure 1 for the general location of these flights). These flights were designed to sample the boundary layer or immediately above, generally at altitudes 2 km AGL or less. We extracted modeled concentrations of trace gases and aerosols along the same latitudes, longitudes, and altitudes, and at the same time as the aircraft flight tracks for a total of 13 flights during 25 Apr – 14 May of the spring IOP1 and a total of 19 flights during 29 Aug – 20 Sep of the summer IOP2. WRF-Chem model outputs were written every 30 minutes for this purpose.

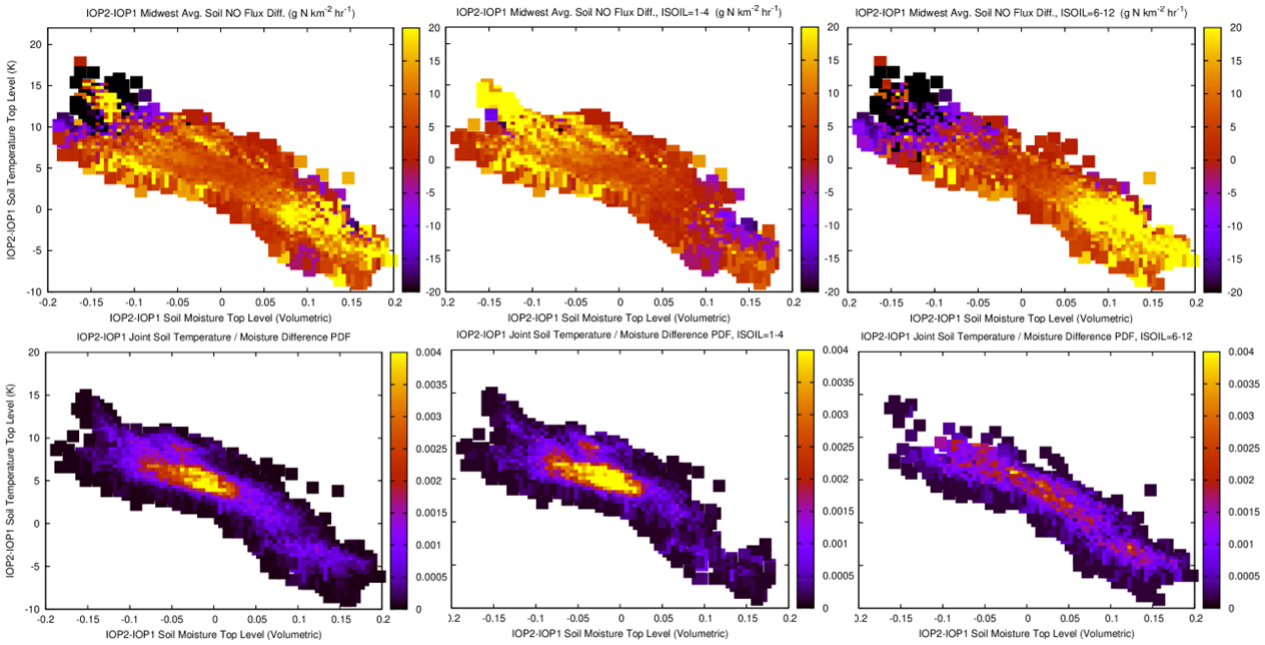

Figure 12. (Top row) Heat map of IOP2 - IOP1 emission differences of soil NO as a function of IOP2 - IOP1 differences of top level soil moisture and temperature; (bottom row) normalized PDF of IOP2 - IOP1 emission differences. Plots are averaged for: (left column) all the Midwest non-agricultural points, (center column) Midwest non-agricultural points for soil types 1-4, (right column) Midwest non-agricultural points for soil types 6-13.

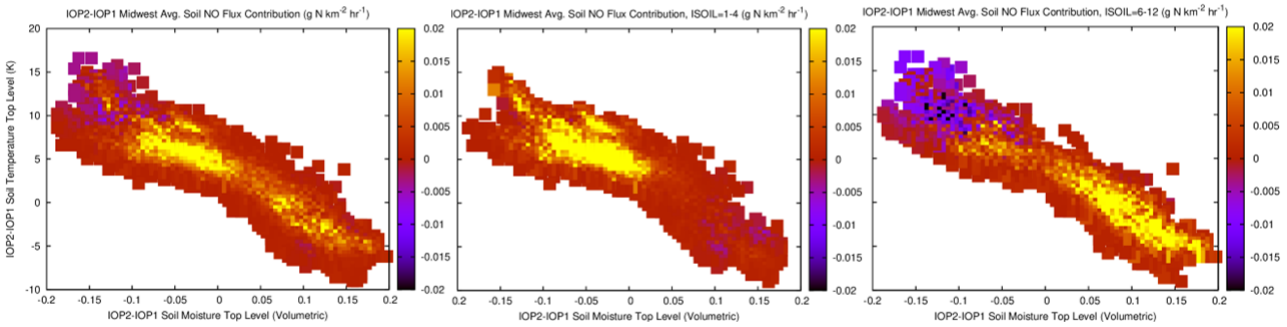

Figure 13. Same as Figure 12, but showing the contribution of each point in the bottom row of Figure 12 to the total IOP2 - IOP1 soil NO flux difference in the top row of Figure 12.

For both IOP1 (Figure 14a) and IOP2 (Figure 15a), the model without soil NO emissions greatly underpredicts NO, while including soil NO brings the model predictions closer to observations, although the model still underpredicts NO. However, the model with soil NO emissions overestimates ozone by a few ppb during both IOPs (Figures 14b and 15b). The causes for the modeled ozone discrepancy are not known at present, although they could range from shortcomings in the chemistry to incorrect predictions of clouds and hence of solar flux, to incorrect specifications of deposition. However, the substantial increase in ozone predicted by the simulation with soil NO compared to without soil NO highlights the strong impact of soil NO emissions on predicted ozone. Thus, the predicted median ozone increases by 5 and 10 ppb during IOP1 and IOP2, respectively (Figures 14b and 15b). Since ozone is NO_x-sensitive in this region (the modeled VOC to NO_x ratio around the SGP central facility is 13 in IOP1 and 18 in IOP2 (not shown)), the high sensitivity of ozone to soil NO emissions is expected and highlights the need to make accurate NO measurements with low detection limits at sub-ppb levels.

Non-refractory aerosol chemical composition was measured using the Aerosol Mass Spectrometer (AMS) onboard the aircraft. The AMS efficiently measures particles below 700 nm aerodynamic diameter, with its aerodynamic lens transmission efficiency dropping sharply above 700 nm diameter (Jayne et al., 2000). Therefore, we only compared the sum of the first two size bins simulated by the model to aircraft AMS data, however, AMS measurements might include some of the larger particles between 700 nm to 1 μm (Jayne et al., 2000). Figure 14c and Figure 15c show that the median and interquartile ranges of the model simulations that include soil NO emissions are closer to observations, while simulations excluding soil NO emissions greatly underpredict the AMS-observed nitrate aerosol. However, even with soil NO emissions, the model underestimates measured nitrate aerosol.

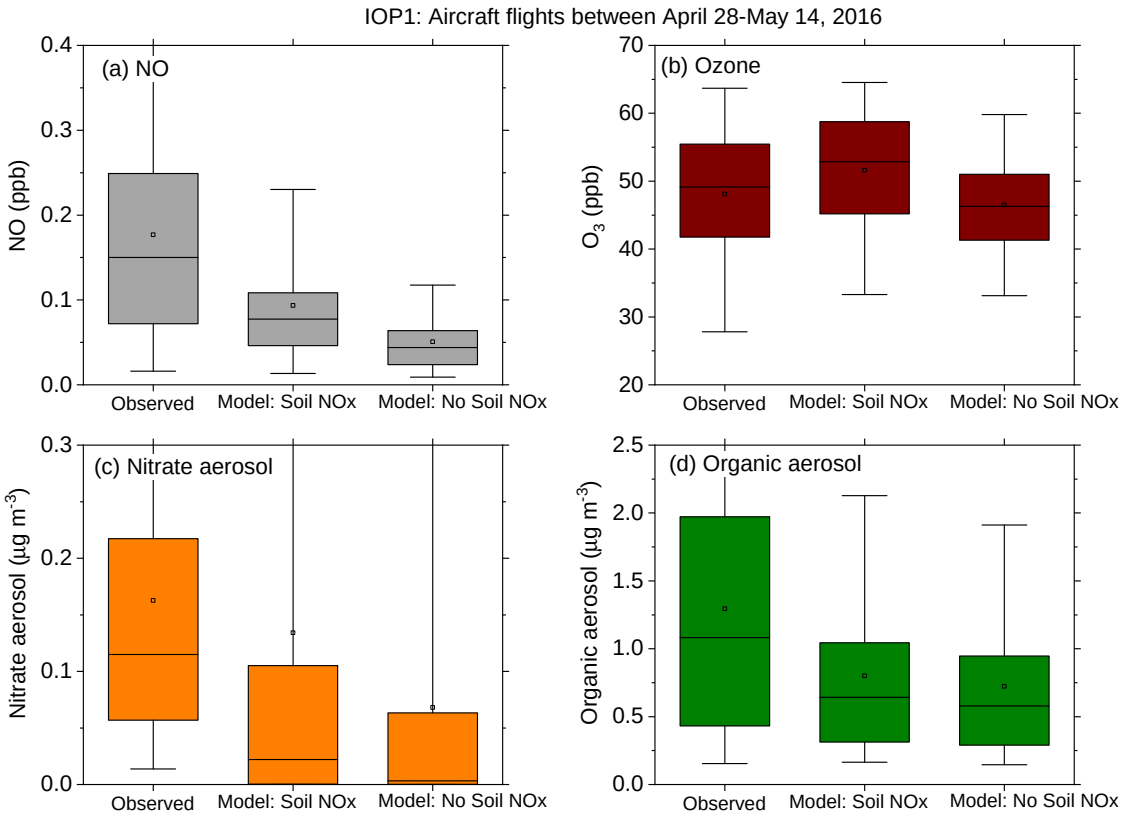

Figure 14. Box and whisker plots of concentrations of (top left) NO, (top right) O_3, (bottom left) nitrate aerosol, and (bottom right) organic aerosol along all IOP1 flight transects in the observations and in model simulations with soil NO_x and without soil NO_x. Open squares indicate mean values.

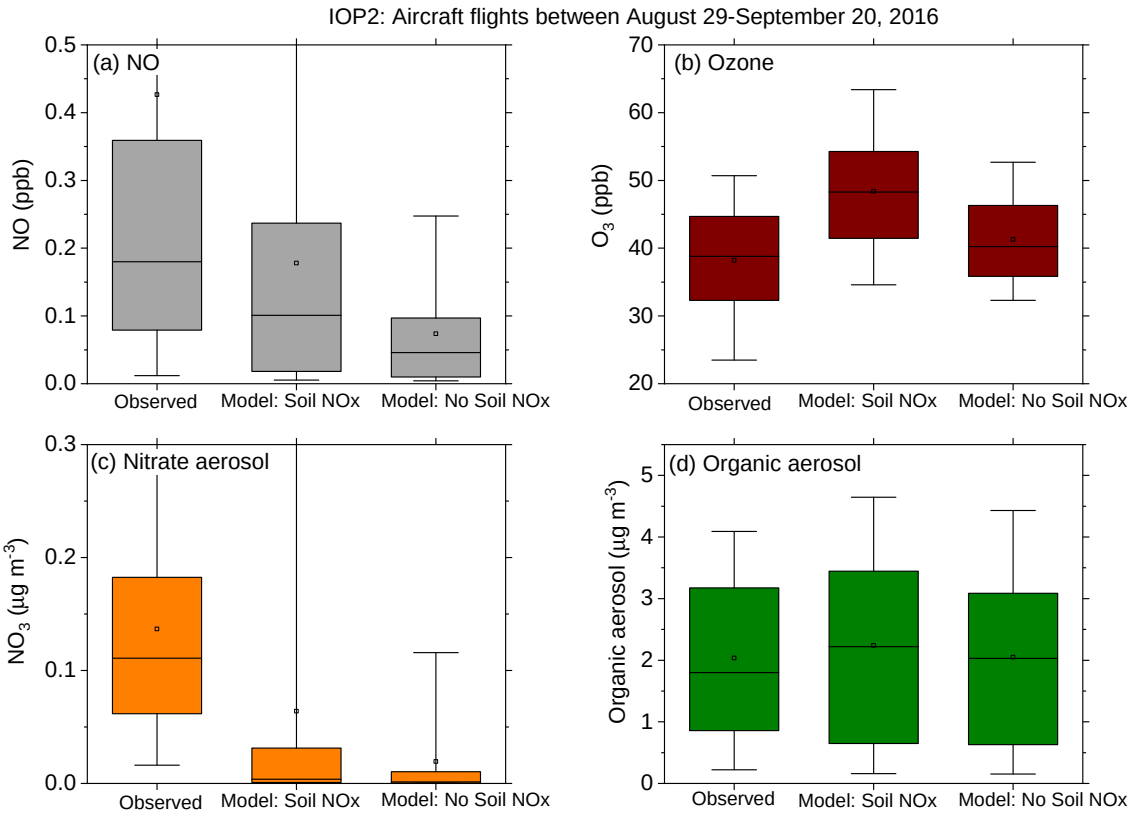

Figure 15. Same as Figure 14, but for IOP2.

Part of the model underprediction might be due to the contribution of particles above 700 nm to nitrate aerosol, which were not included, since size bin 3 in WRF-Chem includes particles from 0.624 to 2.5 μm, while the AMS aerodynamic lens transmission efficiency approaches zero for particles above 1 μm. Note that model predictions suggest that uptake of nitrate on supermicron dust particles is significant (Fairlie et al., 2010; Zaveri et al., 2021). In this work, the model predictions of nitric acid uptake on dust-containing particles were slowed down by reducing the mass accommodation coefficient from a fixed value of 0.1 to a RH-dependent value that ranges from 0.001 at 1% RH (dry) to 0.178 at greater or equal to 90% RH (humid) (Fairlie et al., 2010; Zaveri et al., 2021). Despite this reduction in nitrate uptake on dust particles, WRF-Chem predicts substantial nitrate aerosol in size bin 3 (0.624 to 2.5 μm) and 4 (2.5 to 10.0 μm) that exceeds nitrate aerosols in size bins 1 and 2. As discussed above, part of size bin 3 likely contributes to the model-measurement differences. In addition, the AMS measures total nitrate (organic + inorganic), while the model predictions are just for inorganic nitrate aerosols. Organic nitrates (forming a part of predicted SOA) are implicitly included in WRF-Chem via oxidant and NO_x dependent SOA yield parameterizations (Shrivastava et al., 2011), however, estimating the organic nitrate contribution to simulated SOA is not plausible given the multigenerational aging reactions of SOA precursors with multiple oxidants in the atmosphere (OH, O_3 and NO_3 radicals). Figures 14d and 15d show that soil NO emissions minimally affect predicted total organic aerosols, with simulations including soil NO being higher than those without. While the models (with and without soil NO emissions) underpredict total organic aerosol during IOP1 (median of the models lower by a factor of 2 compared to aircraft observations, Figure 14d), the models moderately overpredict organic aerosols during IOP2 (modeled median is around 25% higher than the observed median, Figure 15d).

In Figure 16 we now compare the concentrations of various species in the SNOx (orange) and NoSNOx (blue) simulations against hourly surface-based Environmental Protection Agency (EPA) measurements (U.S. Environmental Protection Agency, 2024) across several sites in the central U.S. For NO_2 and O_3 we calculate the model's performance with respect to observations in terms of mean normalized bias (MNB), defined by the equation (1).

$$MNB = \frac{1}{n}\sum_{i=1}^{n}\frac{(Mod_i - Obs_i)}{Obs_i} \tag{1}$$

where:

- n is the total number of observations,
- Mod_i is the modeled value at the i^{th} observation,
- Obs_i is the observed value at the i^{th} observation.

The results are binned according to the magnitude of the SNOx - NoSNOx difference in NO concentration. We can see that for NO the concentrations in simulation NoSNOx are consistently too small across all bins. For simulation SNOx, however, the biases, while still generally negative, are closer to zero, especially for bins $> 1-2$ ppb difference. For these bins, we also see that the negative MNB values of O_3 concentration in NoSNOx are also essentially eliminated in simulation SNOx; for the 0-1 ppb difference bin, the ozone concentration is also increased in simulation SNOx relative to NoSNOx, but neither simulation is clearly closer to the observations than the other.

EPA measurements reporting chemical composition of $\mathbf{PM_{2.5}}$ are available at daily intervals. The bottom panel of Figure 16 shows scatterplots of the model (sum of first 3 size bins that encompass aerosol sizes between 0.039 to 2.5 μm) vs. observations. While the scatter about the 1 : 1 lines is quite large for both simulations, we see larger neg-

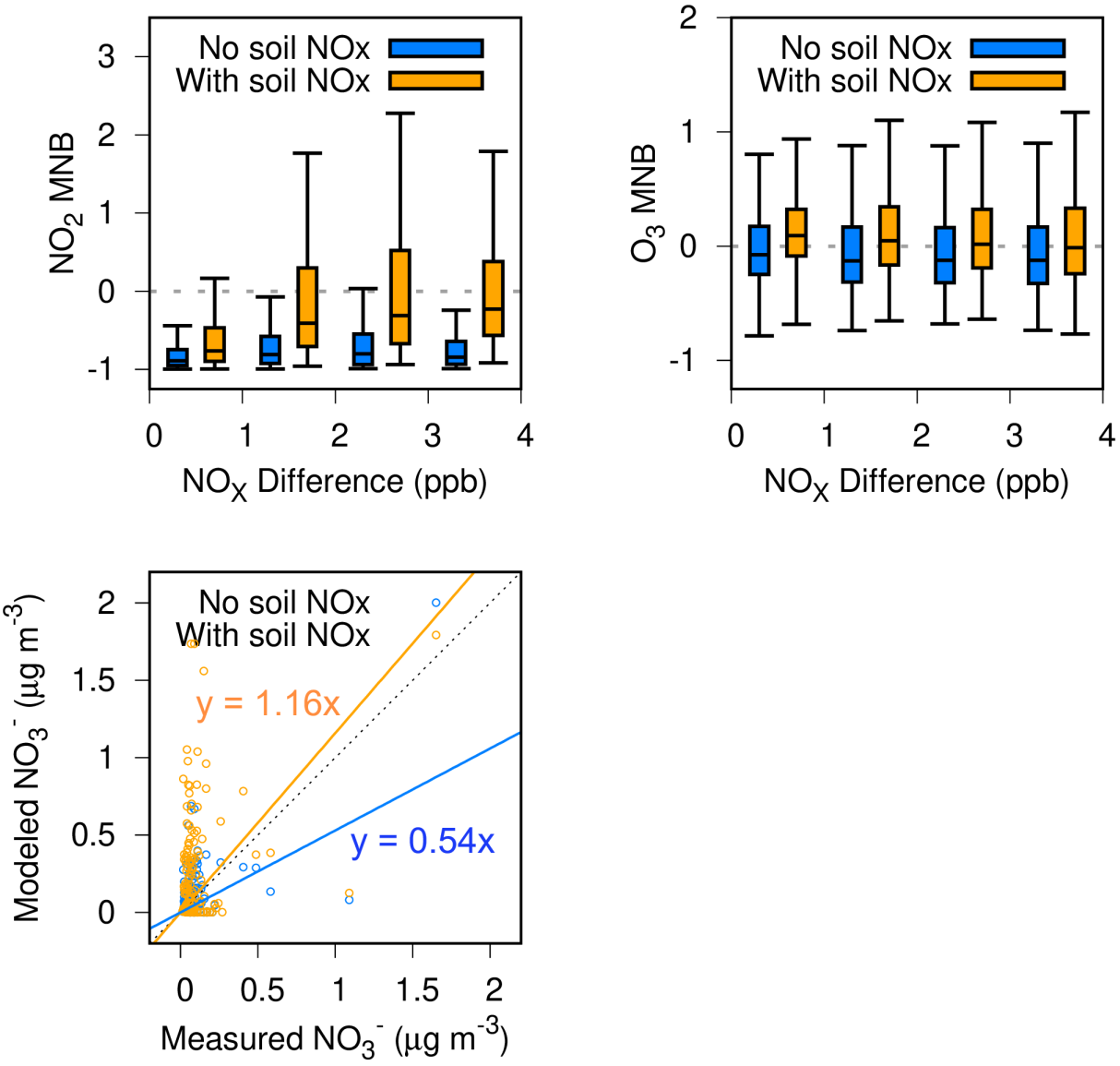

Figure 16. (Top left) Mean normalized bias of NO_2 emissions relative to EPA observations for simulation with soil NO_x (orange) and simulation without soil NO_x (blue), binned by NO_x difference between the simulations. (Top right) Same as top left panel, but for O_3. (Bottom left) Scatterplot of modeled nitrate aerosol mass concentration vs. EPA daily observations for simulation with soil NO_x (orange), and simulation without soil NO_x (blue).

ative biases in nitrate for the NoSNOx simulation (slope of 0.54) that are mitigated in the SNOx simulation (slope of 1.16).

Our results suggest that the inclusion of soil NO emissions improves model performance with respect to measurements of NO gases and nitrate aerosols near the surface. Simulated ozone increases due to soil NO emissions by 5-10 ppb during both IOPs, consistent with NO_x sensitive regime of O_3 due to high VOC/NO_x ratios in the central U.S.

4 Discussion

It is important to note that trends in both soil moisture and soil temperature are important for determining regional-scale soil NO emissions, based on this parameterization. Diurnal variations are governed by soil temperatures changes due to its shorter timescale of variability versus soil moisture; the systematic impact of the higher temperatures during IOP2 versus IOP1 is also important. However, within the Midwest region, spatial variability of soil NO emissions relates to soil moisture patterns as much as, if not more than, soil temperature patterns. This is particularly true for the set of more clay-like soils, where the IOP2 - IOP1 flux patterns run counter to what one would expect from the soil temperature changes.

The strong negative correlation between soil temperature and soil moisture changes across nearly all soil types is likely not a coincidence. It likely reflects the physics of the impact of soil moisture on the surface energy balance (less moisture requires more radiative energy input to be balanced by sensible versus latent heat fluxes, which requires increased soil temperatures). If so, then it shows that soil moisture has strong impacts of soil NO fluxes both directly in the parameterization as well as indirectly, through modulating the soil temperature. However, it is still hard to determine if the soil temperature / moisture correlation physically represents energy balance, or if it simply reflects the fact that most model precipitation between IOP1 and IOP2 occurred in the southern part of the Midwest, whereas most of the warming occurred in the northern part of the Midwest. We should also note that while a soil moisture dataset with 1 km grid spacing was utilized, the actual WRF-Chem simulations were performed at substantially coarser resolution (12 km grid spacing). Simulations performed at higher horizontal resolution (i.e., a few km) could thus be performed using this soil moisture dataset to more fully determine the impact of soil properties on emission variability. Such simulations would also have the benefit of permitting convective clouds to be at least partially resolved, and thus the impact of cloud processing on gases and aerosols cloud be explicitly captured.

The preceding suggests that modeling soil NO fluxes accurately also requires an adequate specification of soil textural mapping and properties. To some degree, the systematic flux differences between IOP1 and IOP2 reflect the coincidence of sandy soils mainly warming / drying while clay soils were cooling / moistening. But Tai et al. (2025) had noted that multiple soil moisture products, including the product developed in that reference used here, had some difficulty representing soil moisture evolution for soils of predominantly clay. Further investigation of this issue is warranted.

5 Conclusions and Future Work

We have successfully implemented a mechanistic soil NO scheme into WRF-Chem and used it within regional scale simulations of the HI-SCALE IOPs to produce reasonable concentrations. We have seen that, when integrated over the Midwest region as we have defined it, the impact of soil NO emissions on the total NO_x concentration can approach the impact of anthropogenic sources at night, amounting to 1-2 ppb. The net impacts on integrated O_3 concentration are up to 5-10 % and 5 ppb, and regionally can approach 10 ppb, which could affect non-attainment status in certain locations. We have seen that the seasonal differences between an Apr-May and an Aug-Sep time period can

potentially impact the total fluxes of soil NO emissions by about 25%. Having unbiased and realistic representations of soil moisture and temperature, as well as other soil properties, is important for modeling these effects properly.

Simulations that include soil NO emissions, at least near the SGP site and more generally over the U.S. Great Plains, have related species concentrations that match better with surface and airborne observations, which tend to have strong negative biases otherwise. So neglecting soil NO emissions may be at least be one factor contributing to biases in chemical species predictions. However, significant model biases in trace gas and aerosol concentrations exist even with the inclusion of soil NO and suggest that other factors, beyond the scope of this study, contribute . More validation of the predictions of the scheme, in terms of soil composition and emissions, should be performed wherever feasible, across a range of geographical conditions. Other factors such as the impacts of agricultural practices and land use modification should also be investigated further for the best regional predictions.

Biases in modeled concentrations might also derive from the representation of chemical processes, such as deposition. One possible source of error might be insufficient representation of VOC emissions and concentrations due to their strong impact on NO_x chemistry, as well as acting as potential precursors of SOA. In addition to local anthropogenic sources, trees can emit VOC species such as isoprene in large quantities depending on the region. New measurements at ARM's Bankhead National Forest site in northern Alabama will provide an opportunity to validate the impact of soil NO emissions in forested regions with a different mix of VOCs, providing further validation of the WRF-Chem setup.

As noted previously, some of the biases might relate to differences in the way different-sized aerosols are binned in the model and observed by the instrumentation. Case studies can be done using WRF-Chem chemistry packages that are more sophisticated than the optimized one used here but too computationally expensive to apply over a whole IOP period. In particular, expanding the number of MOSAIC bins to 8 or more is needed to properly assess the full implication of enhanced NO_x on aerosol size distributions.

Since the presence of soil NO in the model does lead to increasing nitrate aerosol concentrations relative to organic aerosol, which are presumably more hygroscopic and more able to serve as CCN, these emissions thus have the potential to influence the prediction of cloud nucleation and other cloud properties. However, simulations at the cloud resolving scale (few km) would be needed to fully assess this impact. It is also possible that simulations at the cloud resolving scale would also produce better correlations of modeled chemical species with aircraft observations.

Appendix A Soil temperature and moisture dependencies of scheme.

The soil moisture and temperature dependence of the soil NO parameterization largely follow what is described in Rasool et al. (2019b). The rate of nitrification is a product of pH, soil moisture, and soil temperature factors (though the rate is capped below a threshold). The nitrification soil temperature factor is given by:

$$f_{NT} = \max(0.041 \times (T_S - 278.15), 0), \tag{A1}$$

where T_S is the soil temperature in Kelvin. The nitrification soil moisture factor is given by:

$$f_{NM} = \begin{cases} 0.1 & \text{if } M_S \leq W_P \\ \max(0.1, 0.1 + 0.9 \times \sqrt{w_1}, w_2) & \text{if } W_P < M_S < WG_{25} \\ 1.0 & \text{if } WG_{25} < M_S < F_C \\ \max(0.1, 1.0 - w_3) & \text{if } M_S > F_C, \end{cases} \tag{A2}$$

where M_S is the volumetric soil moisture, W_P is the wilting point, F_C is the field capacity, WG_{25} is given by $W_P + 0.25 \times (F_C - W_P)$, $w_1 = (M_S - W_P)/(F_C - W_P)$, $w_2 =$

$(M_S - W_P)/(WG_{25} - W_P)$, and $w_3 = (M_S - F_C)/(SAT - F_C)$, where SAT is the volumetric soil moisture at saturation.

The rate of denitrification also is proportional to a soil temperature and soil moisture factor. The soil temperature factor is not as given by Rasool et al. (2019b), but by the following derived from EPIC:

$$f_{DT} = \max(0.0, (T_S - 273.15)/(T_S - 273.15 + \exp(5.059 - 0.2504 \times (T_S - 273.15)))). \quad \text{(A3)}$$

The denitrification soil moisture factor is a function of water-filled pore space, $WFPS \equiv (M_S - W_{res})/(SAT - W_{res})$, where W_{res} is the soil residual water. For the WRF-Chem implementation $W_{res} = 0$. The factor is then given by:

$$f_{DM} = \min(1.0, \frac{4.82}{(14.0^{16.00/(12.0^{1.39 \times WFPS})})}) \quad \text{(A4)}$$

As noted in the text, WFPS not only directly affects the rate of denitrification itself in the scheme, but it also impacts the soil gas diffusivity, which in turn impacts the ratio of NO_x to N_2O emitted by both nitrification and denitrification.

Open Research Section

The WRF source code used to perform the simulations can be found at the following Zenodo link: https://doi.org/10.5281/zenodo.15103163. The geographical datasets of soil and land use properties used to supplement the WRF static datasets can be found here (Rasool et al., 2019a): https://doi.org/10.3334/ORNLDAAC/1661. The 1-km soil moisture data product used for these simulations (Tai et al., 2024) can be found at the following Zenodo link: https://zenodo.org/records/14370563. Aircraft data were obtained from the Atmospheric Radiation Measurement (ARM) User Facility, a U.S. Department of Energy (DOE) Office of Science user facility managed by the Biological and Environmental Research Program.

Author Contributions

BG implemented the soil emission scheme software from CMAQ into WRF, performed the experimental investigation, analyzed experiments, performed visualization, and wrote original draft. JF conceptualized the research, led funding acquisition, performed project administration, and reviewed draft. QR created methodology of the new soil emission scheme, and software for implementing scheme into CMAQ, created static dataset resources needed for scheme, performed EPIC simulations to provide agricultural input, and reviewed of draft. MS created methodology and software for WRF chemistry, assisted with experimental design, analyzed experiments, validated experiments with flight data, and reviewed and edited draft. ST created soil moisture dataset resources used by scheme and reviewed draft. RZ created methodology and software for WRF chemistry and reviewed draft. JZ analyzed experiments, validated experiments with EPA data, and reviewed draft.

Acknowledgments

This research was supported by the Atmospheric Science Research (ASR) program as part of the DOE Office of Biological and Environmental Research. Pacific Northwest National Laboratory is operated by DOE by the Battelle Memorial Institute under contract DE-AC05-76RL01830. Simulations were performed on PNNL's Research Computing clusters. Ying Liu helped to process the chemical anthropogenic emission and PFT data.

References

Berg, L. K., Shrivastava, M., Easter, R. C., Fast, J. D., Chapman, E. G., Liu, Y., & Ferrare, R. A. (2015). A new wrf-chem treatment for studying regional-scale impacts of cloud processes on aerosol and trace gases in parameterized cumuli. *Geoscientific Model Development*, *8*(2), 409–429. Retrieved from https://gmd.copernicus.org/articles/8/409/2015/ doi: 10.5194/gmd-8-409-2015

Chapman, E. G., Gustafson Jr., W. I., Easter, R. C., Barnard, J. C., Ghan, S. J., Pekour, M. S., & Fast, J. D. (2009). Coupling aerosol-cloud-radiative processes in the wrf-chem model: Investigating the radiative impact of elevated point sources. *Atmospheric Chemistry and Physics*, *9*(3), 945–964. Retrieved from https://acp.copernicus.org/articles/9/945/2009/ doi: 10.5194/acp-9-945-2009

Dowell, D. C., Alexander, C. R., James, E. P., Weygandt, S. S., Benjamin, S. G., Manikin, G. S., ... Alcott, T. I. (2022). The high-resolution rapid refresh (hrrr): An hourly updating convection-allowing forecast model. part i: Motivation and system description. *Weather and Forecasting*, *37*(8), 1371 - 1395. Retrieved from https://journals.ametsoc.org/view/journals/wefo/37/8/WAF-D-21-0151.1.xml doi: 10.1175/WAF-D-21-0151.1

Easter, R. C., Ghan, S. J., Zhang, Y., Saylor, R. D., Chapman, E. G., Laulainen, N. S., ... Zaveri, R. A. (2004). Mirage: Model description and evaluation of aerosols and trace gases. *Journal of Geophysical Research: Atmospheres*, *109*(D20). Retrieved from https://agupubs.onlinelibrary.wiley.com/doi/abs/10.1029/2004JD004571 doi: https://doi.org/10.1029/2004JD004571

Emmons, L. K., Schwantes, R. H., Orlando, J. J., Tyndall, G., Kinnison, D., Lamarque, J.-F., ... Pétron, G. (2020). The chemistry mechanism in the community earth system model version 2 (cesm2). *Journal of Advances in Modeling Earth Systems*, *12*(4), e2019MS001882. Retrieved from https://agupubs.onlinelibrary.wiley.com/doi/abs/10.1029/2019MS001882 (e2019MS001882 2019MS001882) doi: https://doi.org/10.1029/2019MS001882

Fairlie, T. D., Jacob, D. J., Dibb, J. E., Alexander, B., Avery, M. A., van Donkelaar, A., & Zhang, L. (2010). Impact of mineral dust on nitrate, sulfate, and ozone in transpacific asian pollution plumes. *Atmospheric Chemistry and Physics*, *10*(8), 3999–4012. Retrieved from https://acp.copernicus.org/articles/10/3999/2010/ doi: 10.5194/acp-10-3999-2010

Fast, J., Aiken, A. C., Allan, J., Alexander, L., Campos, T., Canagaratna, M. R., ... Zaveri, R. (2009). Evaluating simulated primary anthropogenic and biomass burning organic aerosols during milagro: implications for assessing treatments of secondary organic aerosols. *Atmospheric Chemistry and Physics*, *9*(16), 6191–6215. Retrieved from https://acp.copernicus.org/articles/9/6191/2009/ doi: 10.5194/acp-9-6191-2009

Fast, J., Berg, L. K., Alexander, L., Bell, D., D'Ambro, E., Hubbe, J., ... Zelenyuk, A. (2019). Overview of the hi-scale field campaign: A new perspective on shallow convective clouds. *Bulletin of the American Meteorological Society*, *100*(5), 821 - 840. Retrieved from https://journals.ametsoc.org/view/journals/bams/100/5/bams-d-18-0030.1.xml doi: 10.1175/BAMS-D-18-0030.1

Fast, J., Gustafson Jr., W. I., Easter, R. C., Zaveri, R. A., Barnard, J. C., Chapman, E. G., ... Peckham, S. E. (2006). Evolution of ozone, particulates, and aerosol direct radiative forcing in the vicinity of houston using a fully coupled meteorology-chemistry-aerosol model. *Journal of Geophysical Research: Atmospheres*, *111*(D21). Retrieved from https://agupubs.onlinelibrary.wiley.com/doi/abs/10.1029/2005JD006721 doi: https://doi.org/10.1029/2005JD006721

Grell, G. A., Peckham, S. E., Schmitz, R., McKeen, S. A., Frost, G., Skamarock,

W. C., & Eder, B. (2005). Fully coupled "online" chemistry within the wrf model. *Atmospheric Environment*, *39*(37), 6957-6975. Retrieved from https://www.sciencedirect.com/science/article/pii/S1352231005003560 doi: https://doi.org/10.1016/j.atmosenv.2005.04.027

Guenther, A. B., Jiang, X., Heald, C. L., Sakulyanontvittaya, T., Duhl, T., Emmons, L. K., & Wang, X. (2012). The model of emissions of gases and aerosols from nature version 2.1 (megan2.1): an extended and updated framework for modeling biogenic emissions. *Geoscientific Model Development*, *5*(6), 1471–1492. Retrieved from https://gmd.copernicus.org/articles/5/1471/2012/ doi: 10.5194/gmd-5-1471-2012

Hong, S.-Y., Noh, Y., & Dudhia, J. (2006). A new vertical diffusion package with an explicit treatment of entrainment processes. *Mon. Wea. Rev.*, *134*, 2318–2341.

Hudman, R. C., Moore, N. E., Mebust, A. K., Martin, R. V., Russell, A. R., Valin, L. C., & Cohen, R. C. (2012). Steps towards a mechanistic model of global soil nitric oxide emissions: implementation and space based-constraints. *Atmospheric Chemistry and Physics*, *12*(16), 7779–7795. Retrieved from https://acp.copernicus.org/articles/12/7779/2012/ doi: 10.5194/acp-12-7779-2012

Iacono, M. J., Delamere, J. S., Mlawer, E. J., Shephard, M. W., Clough, S. A., & Collins, W. D. (2008). Radiative forcing by long-lived greenhouse gases: Calculations with the aer radiative transfer models. *Journal of Geophysical Research: Atmospheres*, *113*(D13). Retrieved from https://agupubs.onlinelibrary.wiley.com/doi/abs/10.1029/2008JD009944 doi: https://doi.org/10.1029/2008JD009944

Jaeglé, L., Steinberger, L., Martin, R. V., & Chance, K. (2005). Global partitioning of NOx sources using satellite observations: Relative roles of fossil fuel combustion, biomass burning and soil emissions. *Faraday Discuss.*, *130*(0), 407–423. Retrieved from http://dx.doi.org/10.1039/B502128F (Publisher: The Royal Society of Chemistry) doi: 10.1039/B502128F

Jayne, J. T., Leard, D. C., Zhang, X., Davidovits, P., Smith, K. A., Kolb, C. E., & Worsnop, D. R. (2000). Development of an aerosol mass spectrometer for size and composition analysis of submicron particles. *Aerosol Science and Technology*, *33*(1-2), 49-70. doi: 10.1080/027868200410840

Lawrence, D. M., Oleson, K. W., Flanner, M. G., Thornton, P. E., Swenson, S. C., Lawrence, P. J., ... Slater, A. G. (2011). Parameterization improvements and functional and structural advances in version 4 of the community land model. *Journal of Advances in Modeling Earth Systems*, *3*(1). Retrieved from https://agupubs.onlinelibrary.wiley.com/doi/abs/10.1029/2011MS00045 doi: https://doi.org/10.1029/2011MS00045

Morrison, H., Curry, J. A., & Khvorostyanov, V. I. (2005). A new double-moment microphysics parameterization for application in cloud and climate models. part i: Description. *Journal of the Atmospheric Sciences*, *62*(6), 1665 - 1677. Retrieved from https://journals.ametsoc.org/view/journals/atsc/62/6/jas3446.1.xml doi: 10.1175/JAS3446.1

Oswald, R., Behrendt, T., Ermel, M., Wu, D., Su, H., Cheng, Y., ... Trebs, I. (2013). Hono emissions from soil bacteria as a major source of atmospheric reactive nitrogen. *Science*, *341*(6151), 1233-1235. Retrieved from https://www.science.org/doi/abs/10.1126/science.1242266 doi: 10.1126/science.1242266

Parton, W. J., Holland, E. A., Del Grosso, S. J., Hartman, M. D., Martin, R. E., Mosier, A. R., ... Schimel, D. S. (2001). Generalized model for no and n2o emissions from soils. *Journal of Geophysical Research: Atmospheres*, *106*(D15), 17403-17419. Retrieved from https://agupubs.onlinelibrary.wiley.com/doi/abs/10.1029/2001JD900101 doi: https://doi.org/10.1029/2001JD900101

Pilegaard, K. (2013). Processes regulating nitric oxide emissions from soils. *Philosophical Transactions of the Royal Society B: Biological Sciences*, *368*(1621), 20130126. Retrieved from https://royalsocietypublishing.org/doi/abs/10.1098/rstb.2013.0126 (_eprint: https://royalsocietypublishing.org/doi/pdf/10.1098/rstb.2013.0126) doi: 10.1098/rstb.2013.0126

Rasool, Q. Z., Bash, J. O., & Cohan, D. S. (2019a). *Mechanistic module for soil nitrogen emissions for cmaq model, north america* [dataset]. Oak Ridge TN, USA: ORNL DAC. Retrieved from https://doi.org/10.3334/ORNLDAAC/1661 doi: 10.3334/ORNLDAAC/1661

Rasool, Q. Z., Bash, J. O., & Cohan, D. S. (2019b). Mechanistic representation of soil nitrogen emissions in the Community Multiscale Air Quality (CMAQ) model v 5.1. *Geoscientific Model Development*, *12*(2), 849–878. Retrieved from https://gmd.copernicus.org/articles/12/849/2019/ doi: 10.5194/gmd-12-849-2019

Rasool, Q. Z., Zhang, R., Lash, B., Cohan, D. S., Cooter, E. J., Bash, J. O., & Lamsal, L. N. (2016). Enhanced representation of soil no emissions in the community multiscale air quality (cmaq) model version 5.0.2. *Geoscientific Model Development*, *9*(9), 3177–3197. Retrieved from https://gmd.copernicus.org/articles/9/3177/2016/ doi: 10.5194/gmd-9-3177-2016

Ren, C., Huang, X., Wang, Y., Zhang, L., Zhou, X., Sun, W., ... Wang, T. (2025). Enhanced soil emissions of reactive nitrogen gases by fertilization and their impacts on secondary air pollution in eastern china. *Environmental Science & Technology*, *59*(10), 5119-5130. Retrieved from https://doi.org/10.1021/acs.est.4c12324 (PMID: 40051057) doi: 10.1021/acs.est.4c12324

Schimel, J. P., & Weintraub, M. N. (2003). The implications of exoenzyme activity on microbial carbon and nitrogen limitation in soil: a theoretical model. *Soil Biology and Biochemistry*, *35*(4), 549-563. Retrieved from https://www.sciencedirect.com/science/article/pii/S0038071703000154 doi: https://doi.org/10.1016/S0038-0717(03)00015-4

Seinfeld, J. H., & Pandis, S. N. (2016). *Atmospheric chemistry and physics: from air pollution to climate change*. John Wiley & Sons.

Shrivastava, M., Andreae, M. O., Artaxo, P., Barbosa, H. M. J., Berg, L. K., Brito, J., ... Zhao, C. (2019, March). Urban pollution greatly enhances formation of natural aerosols over the Amazon rainforest. *Nature Communications*, *10*(1), 1046. Retrieved from https://doi.org/10.1038/s41467-019-08909-4 doi: 10.1038/s41467-019-08909-4

Shrivastava, M., Fast, J., Easter, R., Gustafson Jr., W. I., Zaveri, R. A., Jimenez, J. L., ... Hodzic, A. (2011). Modeling organic aerosols in a megacity: comparison of simple and complex representations of the volatility basis set approach. *Atmospheric Chemistry and Physics*, *11*(13), 6639–6662. Retrieved from https://acp.copernicus.org/articles/11/6639/2011/ doi: 10.5194/acp-11-6639-2011

Stauffer, D. R., & Seaman, N. L. (1990). Use of four-dimensional data assimilation in a limited-area model. part i: Experiments with synoptic-scale data. *Mon. Wea. Rev.*, *118*, 1250–1277.

Tai, S.-L., Yang, Z., Gaudet, B., Sakaguchi, K., Berg, L., Kaul, C., ... Fast., J. (2025). A 1 km soil moisture data over eastern conus generated through assimilating smap data into the noah-mp land surface model. *Earth Systems Science Data*. Retrieved from https://doi.org/10.5194/essd-2024-599 doi: 10.5194/essd-2024-599

Tai, S.-L., Yang, Z., Gaudet, B., Sakaguchi, K., Berg, L., Kaul, C. M., ... Fast, J. (2024, December). *A 1 km soil moisture data over eastern continental u.s. generated through assimilating smap data into the noah-mp land sur-*

face model [dataset]. Zenodo. Retrieved from https://doi.org/10.5281/zenodo.14370563 doi: 10.5281/zenodo.14370563

U.S. Environmental Protection Agency. (2024). *EPA AirData.* https://aqs.epa.gov/aqsweb/airdata/download_files.html. (Accessed: 22 December 2024)

Wang, Y., Fu, X., Wang, T., Ma, J., Gao, H., Wang, X., & Pu, W. (2023). Large contribution of nitrous acid to soil-emitted reactive oxidized nitrogen and its effect on air quality. *Environmental Science & Technology*, *57*(9), 3516-3526. Retrieved from https://doi.org/10.1021/acs.est.2c07793 (PMID: 36802547) doi: 10.1021/acs.est.2c07793

Wang, Y., Fu, X., Wu, D., Wang, M., Lu, K., Mu, Y., ... Wang, T. (2021). Agricultural fertilization aggravates air pollution by stimulating soil nitrous acid emissions at high soil moisture. *Environmental Science & Technology*, *55*(21), 14556-14566. Retrieved from https://doi.org/10.1021/acs.est.1c04134 (PMID: 34658233) doi: 10.1021/acs.est.1c04134

Wang, Y., Jacob, D. J., & Logan, J. A. (1998). Global simulation of tropospheric o3-no x -hydrocarbon chemistry: 1. model formulation. *Journal of Geophysical Research: Atmospheres*, *103*(D9), 10713-10725. Retrieved from https://agupubs.onlinelibrary.wiley.com/doi/abs/10.1029/98JD00158 doi: https://doi.org/10.1029/98JD00158

Xia, Y., Mitchell, K., Ek, M., Sheffield, J., Cosgrove, B., Wood, E., ... Mocko, D. (2012). Continental-scale water and energy flux analysis and validation for the north american land data assimilation system project phase 2 (nldas-2): 1. intercomparison and application of model products. *Journal of Geophysical Research: Atmospheres*, *117*(D3). Retrieved from https://agupubs.onlinelibrary.wiley.com/doi/abs/10.1029/2011JD016048 doi: https://doi.org/10.1029/2011JD016048

Yienger, J. J., & Levy II, H. (1995). Empirical model of global soil-biogenic NO emissions. *Journal of Geophysical Research: Atmospheres*, *100*(D6), 11447–11464. Retrieved from https://agupubs.onlinelibrary.wiley.com/doi/abs/10.1029/95JD00370 (_eprint: https://agupubs.onlinelibrary.wiley.com/doi/pdf/10.1029/95JD00370) doi: https://doi.org/10.1029/95JD00370

Zaveri, R. A., Easter, R. C., Fast, J. D., & Peters, L. K. (2008). Model for simulating aerosol interactions and chemistry (mosaic). *Journal of Geophysical Research: Atmospheres*, *113*(D13). Retrieved from https://agupubs.onlinelibrary.wiley.com/doi/abs/10.1029/2007JD008782 doi: https://doi.org/10.1029/2007JD008782

Zaveri, R. A., Easter, R. C., Shilling, J. E., & Seinfeld, J. H. (2014). Modeling kinetic partitioning of secondary organic aerosol and size distribution dynamics: representing effects of volatility, phase state, and particle-phase reaction. *Atmospheric Chemistry and Physics*, *14*(10), 5153–5181. Retrieved from https://acp.copernicus.org/articles/14/5153/2014/ doi: 10.5194/acp-14-5153-2014

Zaveri, R. A., Easter, R. C., Singh, B., Wang, H., Lu, Z., Tilmes, S., ... Rasch, P. J. (2021). Development and evaluation of chemistry-aerosol-climate model cam5-chem-mam7-mosaic: Global atmospheric distribution and radiative effects of nitrate aerosol. *Journal of Advances in Modeling Earth Systems*, *13*(4), e2020MS002346. Retrieved from https://agupubs.onlinelibrary.wiley.com/doi/abs/10.1029/2020MS002346 (e2020MS002346 2020MS002346) doi: https://doi.org/10.1029/2020MS002346

Zhang, L., Li, Q., Wang, T., Ahmadov, R., Zhang, Q., Li, M., & Lv, M. (2017). Combined impacts of nitrous acid and nitryl chloride on lower-tropospheric ozone: new module development in wrf-chem and application to china. *Atmospheric Chemistry and Physics*, *17*(16), 9733–9750. Retrieved from https://acp.copernicus.org/articles/17/9733/2017/ doi: 10.5194/

945 acp-17-9733-2017
946 Zhang, L., Wang, T., Zhang, Q., Zheng, J., Xu, Z., & Lv, M. (2016). Po-
947 tential sources of nitrous acid (hono) and their impacts on ozone: A wrf-
948 chem study in a polluted subtropical region. *Journal of Geophysical*
949 *Research: Atmospheres*, *121*(7), 3645-3662. Retrieved from `https://`
950 `agupubs.onlinelibrary.wiley.com/doi/abs/10.1002/2015JD024468` doi:
951 https://doi.org/10.1002/2015JD024468
952 Zhao, C., Huang, M., Fast, J. D., Berg, L. K., Qian, Y., Guenther, A., ...
953 Warneke, C. (2016). Sensitivity of biogenic volatile organic compounds
954 to land surface parameterizations and vegetation distributions in cali-
955 fornia. *Geoscientific Model Development*, *9*(5), 1959–1976. Retrieved
956 from `https://gmd.copernicus.org/articles/9/1959/2016/` doi:
957 10.5194/gmd-9-1959-2016